

Quantified H I Morphology VII: star-formation and tidal influence on local dwarf H I morphology

B. W. Holwerda^{1*}, N. Pirzkal², W.J.G. de Blok³, and S–L. Blyth⁴

¹ *European Space Agency, ESTEC, Keplerlaan 1, 2200 AG, Noordwijk, the Netherlands*

² *Space Telescope Science Institute, Baltimore, MD 21218, USA*

³ *Netherlands Institute for Radio Astronomy, Schattenberg 1, 9433 TA Zwiggelte, The Netherlands*

⁴ *Astrophysics, Cosmology and Gravity Centre, Department of Astronomy,
University of Cape Town, Private Bag X3, Rondebosch 7701, Republic of South Africa*

Accepted 1988 December 15. Received 1988 December 14; in original form 1988 October 11

ABSTRACT

Scale-invariant morphology parameters applied to atomic hydrogen maps (H I) of galaxies can be used to quantify the effects of tidal interaction or star-formation on the ISM. Here we apply these parameters, Concentration, Asymmetry, Smoothness, Gini, M_{20} , and the G_M parameter, to two public surveys of nearby dwarf galaxies, the VLA-ANGST and LITTLE-THINGS survey, to explore whether tidal interaction or the ongoing or past star-formation is a dominant force shaping the H I disk of these dwarfs.

Previously, H I morphological criteria were identified for ongoing spiral-spiral interactions. When we apply these to the Irregular dwarf population, they either select almost all or none of the population. We find that only the Asymmetry-based criteria can be used to identify very isolated dwarfs (i.e., these have a low tidal indication). Otherwise, there is little or no relation between the level of tidal interaction and the H I morphology.

We compare the H I morphology to three star-formation rates based on either H α , FUV or the resolved stellar population, probing different star-formation time-scales. The H I morphology parameters that trace the inequality of the distribution, the Gini, G_M , and M_{20} parameters, correlate weakly with all these star-formation rates. This is in line with the picture that local physics dominates the ISM appearance and not tidal effects.

Finally, we compare the SDSS measures of star-formation and stellar mass to the H I morphological parameters for all four H I surveys. In the two lower-resolution H I surveys (12"), there is no relation between star-formation measures and H I morphology. The morphology of the two high-resolution H I surveys (6"), the Asymmetry, Smoothness, Gini, M_{20} , and G_M , do show a link to the total star-formation, but a weak one.

Key words: (galaxies:) Local Group galaxies: dwarf galaxies: ISM galaxies: structure
ISM: structure radio lines: ISM

1 INTRODUCTION

It has recently become clear that the ongoing star formation in smaller galactic systems strongly influences the structure of the dwarf system's interstellar matter (ISM), and vice versa (e.g., Weisz et al. 2009). The low-density and -metallicity environment as well as strong effects of feedback

make local dwarfs an outstanding laboratory to understand the physics of star-formation. In addition, Λ CDM predicts the dynamics to be dominated by their dark matter content but this is observationally still debated (e.g., Oh et al. 2011; Swaters et al. 2011).

Dwarf galaxy morphology is related to their environment, as evident from the relation of stellar morphology with tidal index (Weisz et al. 2011a), as is their gas content (Grcevich & Putman 2009). Both strongly point to the

* E-mail: benne.holwerda@esa.int

gas content as the main driver of dwarf morphology. Similarly, Geha et al. (2012) find that all field and central dwarf galaxies have a low fraction of quenched star-formation, i.e. they all have a substantial gas reservoir. This gas is at significantly sub-solar metallicities (Berg et al. 2012) and there is strong evidence for metal loss from supernova (Tremonti et al. 2004; Dalcanton et al. 2007; Bouché et al. 2007; Kirby et al. 2011).

For these reasons, the local sample of low-mass galaxies has been studied extensively using ultra-violet, optical and near-infrared tracer of star-formation (e.g., Hunter et al. 2006; McQuinn et al. 2012a), ISM (Hunter et al. 2012; Ott et al. 2012), and resolved stellar populations (Dalcanton et al. 2009; Weisz et al. 2011a,c). These studies have been made possible by space observatories which allow for observations of stars and dusty ISM with surface brightnesses, and large programs on the Karl. G. Jansky Very Large Array (VLA) which observe the 21cm line of neutral atomic hydrogen (H I).

A key HST program, the ANGST survey (Dalcanton et al. 2009), has observed a large sample of nearby galaxies, mostly dwarfs, uniformly and in unprecedented depth with the Advanced Camera for Surveys (ACS) on the Hubble Space Telescope (HST). To accompany the HST observations, a large VLA program, the VLA-ANGST survey has observed the neutral ISM in great detail (Ott et al. 2012). The star-formation history from the resolved stellar populations' colours and luminosities has already revealed that star-bursts in these galaxies occur stochastically in both time and location (McQuinn et al. 2012b) over the last several hundred Myrs (see also McQuinn et al. 2009, 2010a,b). A second program, LITTLE-THINGS, has observed a different set of nearby dwarfs with Herschel, Spitzer, GALEX and a large program on the VLA.

The present consensus from these programs is that the processes related to star-formation are all inefficient in dwarf galaxies: the star-formation efficiency, the quenching of star-formation, and the interactions between the star-formation and the ISM dynamics (Skillman et al. 2012).

In this series of papers, we have explored the quantified morphology of available H I maps with the common parameters for observed optical or ultra-violet morphology: concentration-asymmetry-smoothness (Conselice 2003), Gini and M_{20} (Lotz et al. 2004) and G_M (Holwerda et al. 2009, 2011a). Recent interest in these morphology parameters has shifted from high-mass spirals and major interaction to more unequal mass interactions (Lotz et al. 2010a), more gas-rich interactions (Lotz et al. 2010b), both of which typically involve dwarf galaxies, and the visibility times of mergers in this parameter space (Lotz et al. 2011). In Holwerda et al. (2011c), we compare the H I morphology to those at other wavelengths for the THINGS sample, noting that the H I and ultraviolet morphologies are closely related, which would make quantified H I morphology a reasonable tracer for interactions. In the next papers of the series, we use the H I morphology to identify mergers (Holwerda et al. 2011d), their visibility time (Holwerda et al. 2011a), and subsequently infer a merger rate from the *WHISP* survey (Holwerda et al. 2011b), as well as identify phenomena unique to cluster members (Holwerda et al. 2011e) and the those H I disks hosting an extended ultraviolet disks (XUV, Holwerda et al. 2012).

In this paper, we explore the H I morphology of low-mass local dwarf galaxies. These have recently been observed in 21cm radio emission (H I) by the VLA-ANGST and LITTLE-THINGS surveys. A third survey is underway to observe the lower mass galaxies in the local volume (the Survey of H I in Extremely Low-mass Dwarfs (SHIELD, Cannon et al. 2011) but we do not include it due to its low spatial resolution ($\sim 20''$ beam). The combined VLA-ANGST and LITTLE-THINGS span a representative selection of the smallest members of the local volume (60 H I maps). The general picture that emerges from these surveys of low-mass galaxies in the local Universe is that the appearance of the H I becomes amorphous with lower masses: there is a progression from disks with spiral structure to mostly featureless rotating disks to a collection of clouds supported by both rotation and dispersion. Our motivation for this study was to explore how much information there still is in the morphology of the H I in these systems. These morphological parameterizations are used to high redshift with HST imaging of distant galaxies, which equally appear less structured beyond $z \sim 2$, i.e., more as a collection of star-forming regions rather than organized in disks with spiral pattern and bulges. We shall compare the H I morphological parameters to indicators of tidal disturbance and star-formation.

While there are many outstanding questions as to the nature of dwarf galaxies and their ISM and star-formation (see Skillman 2010; Skillman et al. 2012), we focus here on two: What is the impact of the star formation on the structure of their ISM? Does star formation induce or quench further star formation?, i.e., does star formation propagate through the host galaxy or is it stochastic?.

The paper is organized as follows: Section 2 describes the data products and sample from the two surveys used for this paper, Section 3 briefly describes the six morphological parameters, Section 4 presents the results, Section 5 compares the H I morphology of all our catalogs to SDSS estimates of star-formation and mass, Section 6 briefly discusses them, and Section 7 lists our conclusions.

2 DATA

The ‘‘Local Irregulars That Trace Luminosity Extremes’’ (LITTLE-THINGS, Hunter et al. 2012) and the VLA-ANGST (Ott et al. 2012) surveys, are close in observational setup to the The H I Nearby Galaxy Survey (THINGS, Walter et al. 2008), the sample for our first paper (Holwerda et al. 2011c). Both surveys were conducted while the VLA transitioned to the Karl G. Jansky Very Large Array. For this paper, we use the robustly-weighted H I surface density maps (RO). These maps are the highest resolution, contain the most small detail, essential for quantified morphology measurements, at the expense of some large-scale faint structure. This trade-off is essential for quantified morphological measurements which are the most sensitive when sampling at sub-kiloparsec physical scales (Lotz et al. 2004), at which point the diffuse large-scale H I emission barely contributes signal in most parameters (see the comparison in Holwerda et al. 2011c).

2.1 LITTLE-THINGS

The LITTLE-THINGS sample (Hunter et al. 2012) is made up of 42 dwarf irregular (dIm) and Blue Compact Dwarf (BCD) galaxies. The H I observations are a mix of new (21 galaxies) and archival observations. Some galaxies were dropped from the sample due to issues with individual observations. The LITTLE-THINGS sample was drawn from a larger multi-wavelength effort (Hunter & Elmegreen 2004, 2006) and there are extensive ancillary data available for the full sample. Observational setup was kept identical to the THINGS survey (Walter et al. 2008) and data is public at <https://science.nrao.edu/science/surveys/littlethings/>. We converted the the LITTLE-THINGS moment 0 maps into column density maps using the expression in Walter et al. (2008), their equation 5, and the major and minor axes from Hunter et al. (2012) to conform to the VLA-ANGST data products. Typical resolution is slightly lower than VLA-ANGST ($\sim 6\text{-}10''$), depending on the observational configuration.

2.2 VLA-ANGST

The VLA-ANGST sample is based on the volume-limited ANGST survey (Dalcanton et al. 2009). The galaxies in these surveys drawn from the local volume compilation from Karachentsev et al. (2004). This catalog lists relevant parameters and, of specific interest, the tidal index Θ (see §4.1). The ANGST survey targets the local volume, mostly less than 3.5 Mpc away with a limiting distance of 4 Mpc, in order to resolve low-level star-formation from resolved stellar populations. From the 89 ANGST galaxies, VLA-ANGST is a subset of 29 detected galaxies, excluding southern objects and those with no single-dish H I detections or low star-formation. All VLA-ANGST galaxies were observed in both high spatial ($\sim 6''$, corresponding to ~ 100 pc) and spectral (corresponding to 0.65-2.6 km/s in velocity) resolution in the VLA B, C, and D array configurations. For this study, the high velocity resolution is not pertinent but the spatial resolution and depth comparable to the THINGS survey are. Data are available at <https://science.nrao.edu/science/surveys/vla-angst/> and described in detail in Ott et al. (2012) and Warren et al. (2012) presents the H I profiles for these galaxies.

2.3 Final Sample

Some of the H I observations for LITTLE-THINGS are not yet archived and there is some overlap with the VLA-ANGST and LITTLE-THINGS surveys with galaxies included under a different name. Omitted galaxies are NGC1156, NGC6822, DDO6, KDG63, HS117, NGC4190, DDO113, DDO125 DDO181 and DDO183. The galaxies CVnIdwA (UGCA292), GR 8 (DDO155) and UGC 8508 are in both the LITTLE-THINGS and VLA-ANGST surveys. The final tally of H I maps is 60 galaxies.

As noted, the sampling of the two surveys is slightly different: the mean LITTLE-THINGS beam is $7''.2 \times 8''.8$ and the VLA-ANGST one $6''.1 \times 7''.4$ but these resolutions are comparable in the sampling of the H I disk (Figure 1) and the two surveys can be treated as a single data-set.

Table 1. The spatial resolution for the Robustly Weighted column density maps from the LITTLE-THINGS and VLA-ANGST surveys. Information from Hunter et al. (2012) and Ott et al. (2012).

Galaxy	Beam Size		Survey
	Minor	Major	
CVnIdwA	10.5	10.9	LITTLE-THINGS
DDO 43	6.0	8.1	LITTLE-THINGS
DDO 46	5.2	6.3	LITTLE-THINGS
DDO 47	9.0	10.4	LITTLE-THINGS
DDO 50	6.1	7.0	LITTLE-THINGS
DDO 52	5.2	6.8	LITTLE-THINGS
DDO 53	5.7	6.3	LITTLE-THINGS
DDO 63	6.0	7.8	LITTLE-THINGS
DDO 69	5.4	5.8	LITTLE-THINGS
DDO 70	13.2	13.8	LITTLE-THINGS
DDO 75	6.5	7.5	LITTLE-THINGS
DDO 87	6.2	7.6	LITTLE-THINGS
DDO 101	7.0	8.3	LITTLE-THINGS
DDO 126	5.6	6.9	LITTLE-THINGS
DDO 133	10.8	12.4	LITTLE-THINGS
DDO 154	6.3	7.9	LITTLE-THINGS
DDO 155	10.1	11.3	LITTLE-THINGS
DDO 165	7.6	10.0	LITTLE-THINGS
DDO 167	5.3	7.3	LITTLE-THINGS
DDO 168	5.8	7.7	LITTLE-THINGS
DDO 187	5.5	6.2	LITTLE-THINGS
DDO 210	8.6	11.7	LITTLE-THINGS
DDO 216	15.4	16.2	LITTLE-THINGS
IC 10	5.5	5.9	LITTLE-THINGS
IC 1613	6.5	7.7	LITTLE-THINGS
LGC 3	9.3	11.8	LITTLE-THINGS
M81dwA	6.3	7.8	LITTLE-THINGS
NGC 1569	5.2	5.9	LITTLE-THINGS
NGC 2366	5.9	6.9	LITTLE-THINGS
NGC 3738	5.5	6.3	LITTLE-THINGS
NGC 4163	5.9	9.7	LITTLE-THINGS
NGC 4214	6.4	7.6	LITTLE-THINGS
SagDIG	16.9	28.2	LITTLE-THINGS
UGC 8508	4.9	5.9	LITTLE-THINGS
WLM	5.1	7.6	LITTLE-THINGS
Haro 29	5.6	6.8	LITTLE-THINGS
Haro 36	5.8	7.0	LITTLE-THINGS
Mrk 178	5.5	6.2	LITTLE-THINGS
VIIZw 403	7.7	9.4	LITTLE-THINGS

3 QUANTIFYING MORPHOLOGY

We use the Concentration-Asymmetry-Smoothness parameters (CAS, Conselice 2003), combined with the Gini- M_{20} parameters from Lotz et al. (2004), and our own G_M . We have discussed the definitions of these parameters in the previous papers, as well as how we estimate uncertainties for each. Here, we will give a brief overview but for details we refer the reader to Holwerda et al. (2011c,d) or Holwerda et al. *submitted*.

We select pixels in an image as belonging to the galaxy based on the outer H I contour ($5. \times 10^{19}$ atoms/cm²) and adopt the position from the respective survey catalogs as the central position of the galaxy (as reported in Hunter et al. 2012; Ott et al. 2012, respectively). Given a set of n pixels in each object, iterating over pixel i with value I_i ,

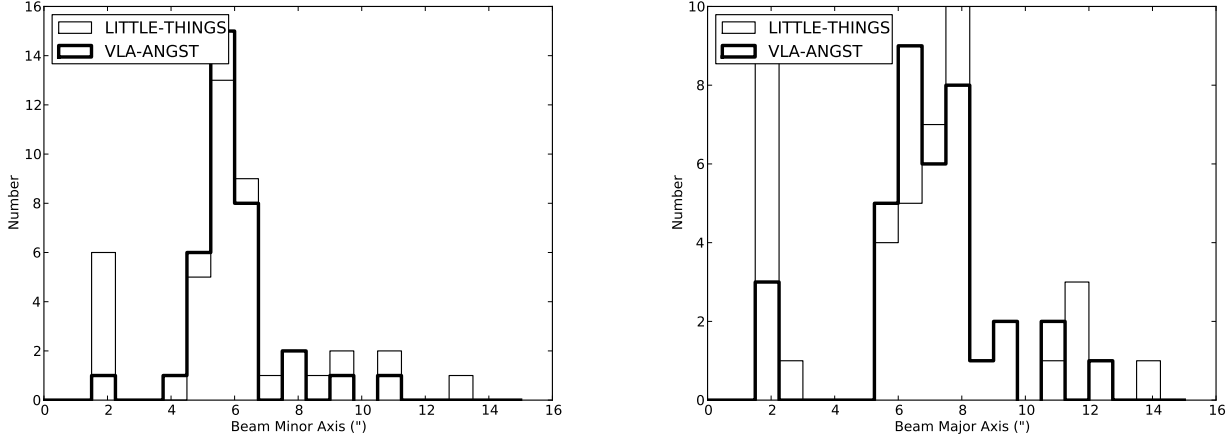


Figure 1. The distribution of minor and major axes of the LITTLE-THINGS and VLA-ANGST H I observations.

Galaxy	Beam Size Minor	Survey Major	
NGC 247	6.2	9.0	VLA-ANGST
DDO 6	6.3	7.2	VLA-ANGST
NGC 404	6.1	7.1	VLA-ANGST
KKH37	5.8	6.5	VLA-ANGST
UGC 4483	5.7	7.6	VLA-ANGST
KK 77	5.8	6.1	VLA-ANGST
BK3N	5.8	6.3	VLA-ANGST
AO0952+69	5.9	6.4	VLA-ANGST
Sextans B	7.5	9.5	VLA-ANGST
NGC 3109	5.0	7.6	VLA-ANGST
Antlia	9.6	10.5	VLA-ANGST
KDG 63	6.0	6.2	VLA-ANGST
Sextans A	6.0	7.3	VLA-ANGST
HS 117	6.1	8.6	VLA-ANGST
DDO 82	5.7	5.8	VLA-ANGST
KDG 73	5.6	6.9	VLA-ANGST
NGC 3741	4.8	5.5	VLA-ANGST
DDO 99	5.2	7.7	VLA-ANGST
NGC 4163	5.4	7.6	VLA-ANGST
NGC 4190	5.3	6.1	VLA-ANGST
DDO 113	7.7	9.9	VLA-ANGST
MCG +09-20-131	5.3	6.1	VLA-ANGST
DDO 125	5.4	6.3	VLA-ANGST
UGCA 292	5.0	7.0	VLA-ANGST
GR 8	5.4	5.8	VLA-ANGST
UGC 8508	6.4	8.2	VLA-ANGST
DDO 181	5.5	7.6	VLA-ANGST
DDO 183	6.2	7.6	VLA-ANGST
KKH 86	5.8	7.5	VLA-ANGST
UGC 8833	11.2	12.4	VLA-ANGST
KKH 230	5.2	5.9	VLA-ANGST
DDO187	5.7	7.1	VLA-ANGST
DDO 190	9.9	10.8	VLA-ANGST
KKR 25	4.4	5.5	VLA-ANGST
KKH 98	5.2	6.2	VLA-ANGST

pixel position x_i, y_i with the centre of the object at x_c, y_c these parameters are defined as:

$$C = 5 \log(r_{80}/r_{20}), \quad (1)$$

with r_f as the radial aperture, centered on x_c, y_c containing

percentage f of the light of the galaxy (see definitions of r_f in Bertin & Arnouts 1996; Holwerda 2005)¹. This concentration index can be used to quickly discern between light profiles; a de Vaucouleurs profile ($I \propto R^{-4}$) has Concentration value of $C = 5.2$, and a purely exponential one has a value of $C = 2.7$. It also can be used to identify unique phenomena, for for example HI disk stripping (Holwerda et al. 2011e).

$$A = \frac{\sum_i |I_i - I_{180}|}{\sum_i |I(i)|}, \quad (2)$$

where I_{180} is the pixel at position i in the galaxy's image, after it was rotated 180° around the centre of the galaxy. Fully symmetric galaxies have very low values of Asymmetry. A regular spiral need not show a high value of Asymmetry, e.g., a grand-design spiral galaxy's spiral arms map onto each other with a 180° rotation (the rotational symmetry of galaxies can be used to infer dust extinction in pairs of galaxies, see White & Keel 1992; White et al. 2000; Domingue et al. 2000; Keel & White 2001a,b; Holwerda et al. 2007; Keel et al. 2013; Holwerda et al. 2013; Holwerda & Keel 2013). Flocculant spirals can be expected to be slightly more Asymmetric still. The highest values of Asymmetry can be found in galaxies with strong tidal disruptions, provided the tidal structures are included in the calculation, which they are in H I.

$$S = \frac{\sum_{i,j} |I(i,j) - I_S(i,j)|}{\sum_{i,j} |I(i,j)|}, \quad (3)$$

where I_S is pixel i in a smoothed image. The type of smoothing (e.g., boxcar or Gaussian) has changed over the years. We chose a fixed $5''$ Gaussian smoothing kernel for simplicity. We note that we use the term "Smoothness" for historical reasons as this has become the de facto designation of this parameter (the CAS scheme), even though an increase in its value means a more clumpy appearance of the image

¹ We must note that the earlier version of our code contained an error, artificially inflating the concentration values. A check revealed this to be $C_{new} = 0.38 \times C_{old}$, and we adopt the new, correct values in this paper.

(hence its original designation "clumpiness"). Very smooth galaxies have very low values of Smoothness but in other galaxies, the value of the Smoothness parameter depends on the size of the smoothing kernel used. If the kernel's size correspond to, for example, the width of spiral arms at the distance of the galaxy, then grand design spirals will have relatively high Smoothness values.

The Gini coefficient is defined as:

$$G = \frac{1}{\bar{I}n(n-1)} \sum_i (2i - n - 1) I_i, \quad (4)$$

where the list of n pixels was first ordered according to value and \bar{I} is the mean pixel value in the image.

Lotz et al. (2004) introduce the relative second-order moment (M_{20}) of an object. The second-order moment of a pixel is: $M_i = I_i \times R_i = I_i \times [(x_i - x_c)^2 + (y_i - y_c)^2]$. The total second-order moment of an image is defined as:

$$M_{tot} = \sum M_i = \sum I_i [(x_i - x_c)^2 + (y_i - y_c)^2] \quad (5)$$

The relative second-order moment of the brightest 20% of the flux:

$$M_{20} = \log \left(\frac{\sum_i^k M_i}{M_{tot}} \right), \text{ for which } \sum_i^k I_i < 0.2 I_{tot} \text{ is true.} \quad (6)$$

where pixel k marks the top 20% point in the flux-ordered pixel-list. The M_{20} parameter is a parameter that is sensitive to bright structure away from the center of the galaxy: flux is weighted in favor of the outer parts. It therefore is relatively sensitive to tidal structures.

Instead of using the intensity of pixel i , the Gini parameter can be defined using the second order moment:

$$G_M = \frac{1}{\bar{M}n(n-1)} \sum_i (2i - n - 1) M_i, \quad (7)$$

These parameters trace different structural characteristics of a galaxy's image but these do not span an orthogonal parameter space (see also the discussion in Scarlata et al. 2007, Holwerda et al. *in preparation*). Two crucial input parameters for the computation of the morphology are the central position (x_c and y_c) and the threshold for including pixels into the calculations. We use the positions reported by Ott et al. (2012) for the VLA-ANGST galaxies and those in the NED database for the LITTLE-THINGS galaxies for the central pixel position. To determine which pixels to include, we adopt a threshold of 5×10^{19} atoms/cm², the practical limiting depth of both of these surveys.

Holwerda et al. (2011c) discuss the uncertainties in these parameters in detail. To estimate their errors, we both vary the input central position and compute the rms from the resulting spread in values. Secondly, we scramble the pixels (but keep the central position identical) to assess the effect of random noise. Thirdly, in the case of the Gini parameter, there is no dependence on the central position. In this case we compute the variance by sub-sampling the pixel collection.

3.1 Spatial Sampling

Interferometric radio observations filter out large-scale faint emission, a unique feature with respect to the characterization of morphology. To remedy this, the total-power information from short baseline observations are needed, i.e., a

Table 2. The different morphological parameters for NGC 3109.

Parameter	VLA-ANGST	KAT-7	inner contour (32Jy/Beam)
C	0.0 ± 0.010	0.20 ± 0.02	0.20 ± 0.08
A	1.0 ± 0.000	1.0 ± 0.0	1.00.0
S	0.047 ± 0.031	0.22 ± 0.09	0.38 ± 0.16
G	0.445 ± 0.010	0.68 ± 0.01	0.23 ± 0.11
M_{20}	-0.741 ± 0.002	-0.71 ± 0.02	-0.70 ± 0.019
G_M	0.429 ± 0.011	0.67 ± 0.01	0.22 ± 0.11

large single-dish telescope or a radio array more compact than the VLA-A configuration.

Fortunately, one of these galaxies, NGC 3109, was observed with the Karoo Array Telescope (KAT-7), a seven-dish precursor array to the MeerKAT telescope (Booth et al. 2009; Jonas 2007; de Blok et al. 2009). These observations and results are described in detail in Carignan et al. (2013). The resulting HI map is sensitive to larger scale HI features such as wide tidal tails or warps. Figure 2 shows both HI maps to illustrate the lack of large-scale, diffuse emission in VLA observations. For example, Carignan et al. (2013) note that the *total* HI mass estimated from the KAT-7 observations agrees well with single-dish observations which do not resolve out any structure.

Figure 2 shows how the KAT-7 observations reveal a pronounced warp in the edge-on HI disk while this is only visible as a slight dip in the VLA data. The question remains if the addition of an additional diffuse level will change the global morphology parameters or if their value is mostly determined by the morphological detail in the VLA data.

We ran our morphological code on the KAT-7 image twice, delineated by different contours, one similar to the area covered by the VLA-ANGST outer contour and one defining the limit of the diffuse emission. Table 2 lists the resulting parameters. There are notable differences between the VLA and KAT-7 observations, to both the outer contour as well as an area corresponding to the VLA-ANGST outer contour.

The differences between the two KAT-7 contours are noticeable in S, G and G_M . The inclusion of a large number of low-intensity pixels will result in a completely different distribution and hence Gini and G_M parameters. The higher range in contrast results in a higher Smoothness –meaning a clumpier image– compared to just the inner contour.

Comparing the inner contour in the KAT-7 observations and the VLA-ANGST observations (second and fourth column in Table 2), we note differences in C, S, G, and to a lesser extend M_{20} and G_M .

The majority of morphological parameters are modified if we change spatial resolution, especially sampling over areas greater than a kpc. The addition of a large-scale structure only changes the measures of (in)equality in the distribution: Gini and G_M . Thus, while large-scale structure is missed by VLA interferometric surveys such as LITTLE-THINGS and VLA-ANGST, most of the morphological information is contained in the small-scale structures that are resolved by such observations.

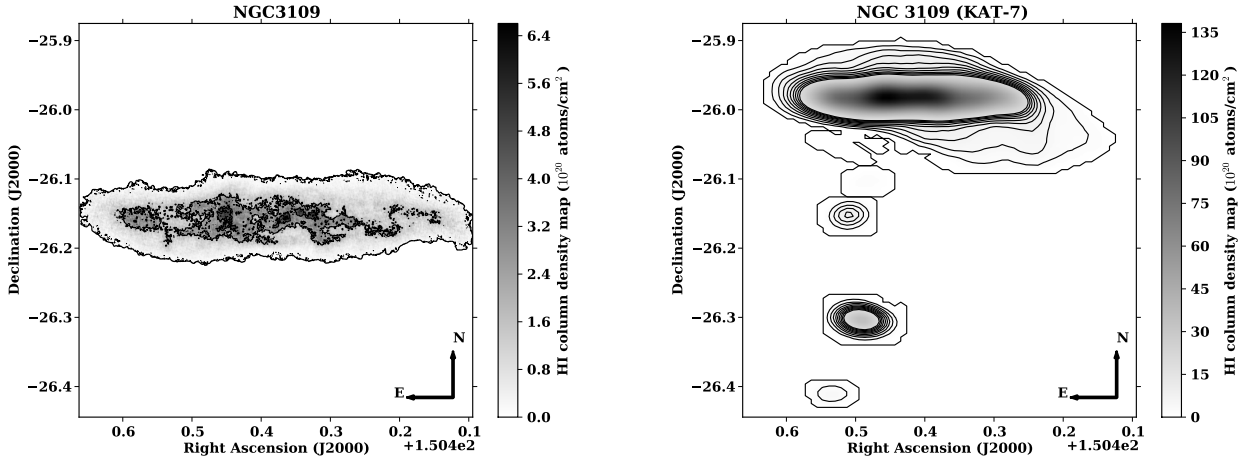


Figure 2. The H I map of NGC 3109 from the VLA-ANGST survey (Ott et al. 2012) and the KAT-7 observations (Carignan et al. 2013), which include several smaller, unresolved galaxies. The outer VLA-contour corresponds to the inner one (32Jy/Beam) for the KAT-7 mosaic. While there is substantial information in the outer regions, their weight in flux is minimal.

4 RESULTS

To explore the relationships between the H I morphological parameters and the tidal and star-formation tracers, we show two plots, one where we compare H I parameters against each other, colour-coded with a comparison parameter, if available. This is to identify possible sections of H I morphology parameter space where special cases reside.

Secondly, we plot the comparison parameter (e.g., a star-formation measure) against the six H I morphological parameters directly and, thirdly, we calculate the Spearman ranking (-1 perfectly anti-correlated, 0 uncorrelated, and 1 fully correlated) between the comparison parameter and H I morphological parameter.

The LITTLE-THINGS sample was drawn from Hunter & Elmegreen (2004) and the VLA-ANGST from Karachentsev et al. (2004), meaning that the parameters on tidal effect or star-formation from the literature are not available for our full sample. We compare the H I morphology to the tidal disturbance, and several parameterizations of the ongoing and past star-formation, to explore which of these are the dominant factor in the overall shape of the H I in these dwarf galaxies.

4.1 Tidal Index

Figure 4 shows the distribution of H I column density map morphologies, coded by the tidal parameter (Θ) from Karachentsev et al. (2004). Figure 3 shows the direct relation between the six H I morphological parameters and the tidal parameter. Of all the parameters, only H I Asymmetry is weakly related to Θ (see also Table 3). The six morphological criteria for interaction of more massive galaxies are denoted with dashed lines in Figure 4 and further.

These criteria are:

$$A > 0.38 \text{ and } S > A \quad (8)$$

from Conselice (2003). This is the straight dashed line in sub-panels (d), (e) and (f) in Figure 4 etc.

Lotz et al. (2004) added two different criteria, one using Gini and M_{20} :

$$G > -0.115 \times M_{20} + 0.384 \quad (9)$$

shown by the dashed line in sub-panel (b) in Figure 4.

Lotz et al. (2004) also defined a interaction criterion based on Gini and Asymmetry:

$$G > -0.4 \times A + 0.66 \text{ or } A > 0.4. \quad (10)$$

which is shown as an inclined dashed line in sub-panel (d) in Figure 4. This latter criterion is a refinement of the Conselice et al. A-S criterion in equation 8.

Holwerda et al. (2011d) defined three interaction criteria specifically for H I data (typically lower spatial resolution, affected by spatial filtering (i.e., sensitivity to a specific angular scale), and smaller dynamical range than optical data). Ongoing spiral-spiral tidal interactions can be identified by:

$$G_M > 0.6, \quad (11)$$

which is not shown in Figure 4 as the range of G_M values in the Dwarf galaxy H I surveys does not extend this high. However, it is shown as the vertical dashed line in sub-panels (a), (c), (f) and (j) in Figures 21, 23 and 25.

Or their interaction can be identified based on Asymmetry and M_{20} :

$$A > -0.2 \times M_{20} + 0.25, \quad (12)$$

or concentration and M_{20} , similar to the criteria from Lotz et al. (2004) (equations 9 and 10), as:

$$C_{82} > -5 \times M_{20} + 3. \quad (13)$$

The first thing we note, is that the vast majority of dwarfs galaxies lie on one side of these criteria. The G-A and G- M_{20} criteria include almost all; the C- M_{20} and G_M criteria both completely exclude the dwarf from the tidally interacting. Only the Gini- M_{20} criterion bisects the dwarf sample. If we compare these criteria to the values of the tidal index Θ , there is little correlation with the position in H I morphology parameter space. The exception are three

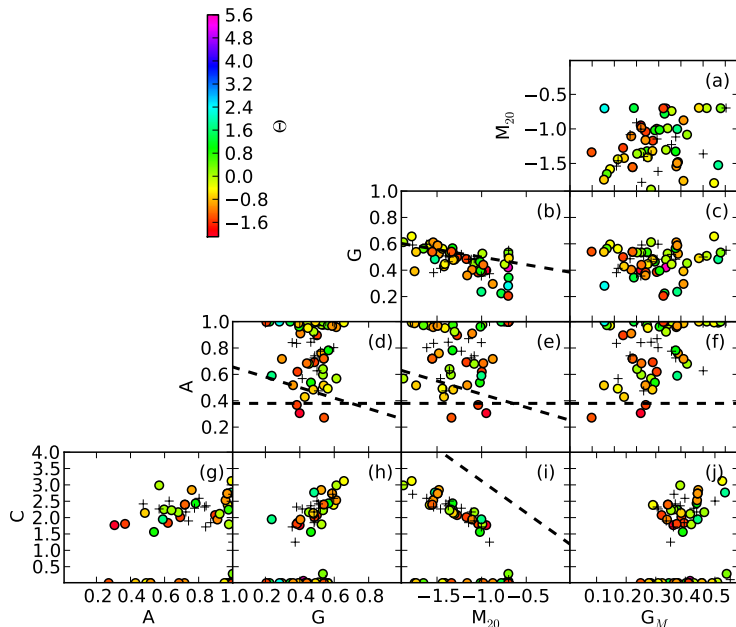


Figure 4. The distribution of the H I morphological parameters with the tidal index Θ from Karachentsev et al. (2004). Dashed lines are the criteria for major interaction from Holwerda et al. (2011a), based on the WHISP sample or established morphological selections of mergers in optical data. Values of the tidal index appear poorly related to the position of the dwarfs in H I morphology space. Only very isolated dwarfs ($\Theta < -1$) are also very symmetric in H I ($A < 0.4$), the H I parameter with the highest correlation with tidal index (Table 3).

galaxies with low values of Θ , i.e. very isolated, and a low asymmetry value ($A < 0.4$).

Figures 3 and 4 show that the H I morphology is not primarily affected by the gravitational interaction. One can identify very isolated galaxies from the H I morphology ($A < 0.4$) but the majority of criteria that apply to spiral galaxies cannot be applied to dwarf H I morphology to identify or even rank the level of interaction. We identify DDO47, DDO87, and UGC8833 as the most isolated dwarfs in our sample, based on their Asymmetry.

4.2 Ongoing and Past Star-Formation

The star-formation can be measured by a variety of techniques corresponding to different typical timescales: (a) H α emission which traces the currently forming massive stars still in their ionized birth clouds (tens of Myr), (b) far-ultraviolet (FUV) emission which traces the population of massive young stars, after the surrounding gas has dissipated (hundreds of Myr), and (c) resolved stellar populations which trace the star-formation history to Gyr timescales.

Here we compare the H I morphologies to these three star-formation tracers to explore which time-scale of star-formation informs the morphology of the atomic gas: current from H α emission, reported in Hunter et al. (2006), recent from FUV fluxes, reported in Hunter et al. (2010) and McQuinn et al. *in preparation*, or long-term star-formation history from HST resolved stellar populations, reported in Weisz et al. (2011a) and McQuinn et al. (2012a).

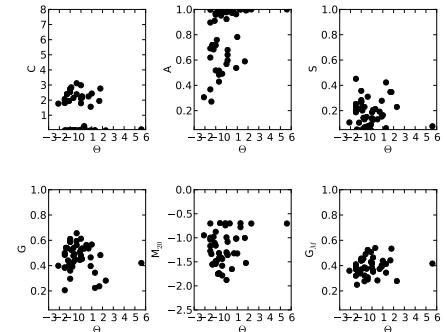


Figure 3. The six H I morphology parameters as a function of the tidal parameter Θ from Karachentsev et al. (2004). $\Theta = 0$ is undisturbed, a negative value means residing in an under-density and a positive one means increased tidal influence by neighbouring systems.

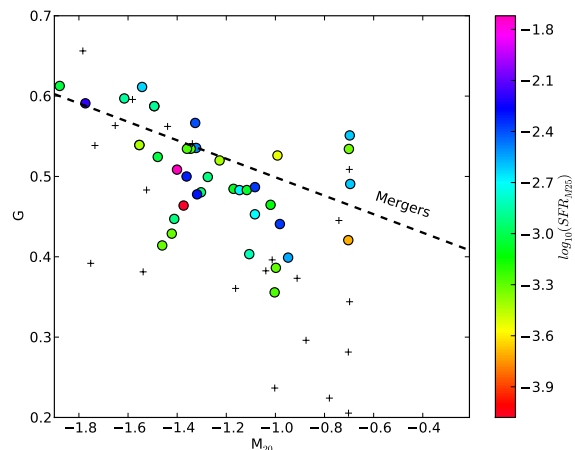


Figure 9. The M_{20} and Gini parameters of the H I maps colour coded by the star-formation surface density over the optical disk ($\log_{10}(SFR_{M25})$) from Hunter & Elmegreen (2004). The dashed line is a criterion for major interaction from Holwerda et al. (2011a); Lotz et al. (2004).

4.2.1 Current Star-Formation: $SFR_{H\alpha}$

Figure 6 shows the distribution of H I column density map morphologies, coded by their *total* star-formation, inferred from H α flux from Hunter & Elmegreen (2004), their Table 3. Typical low star-formation rates from H α flux values ($SFR_{H\alpha} \sim -2.8$) are found predominantly in low H I Asymmetry galaxies. They also suggestively cluster else-

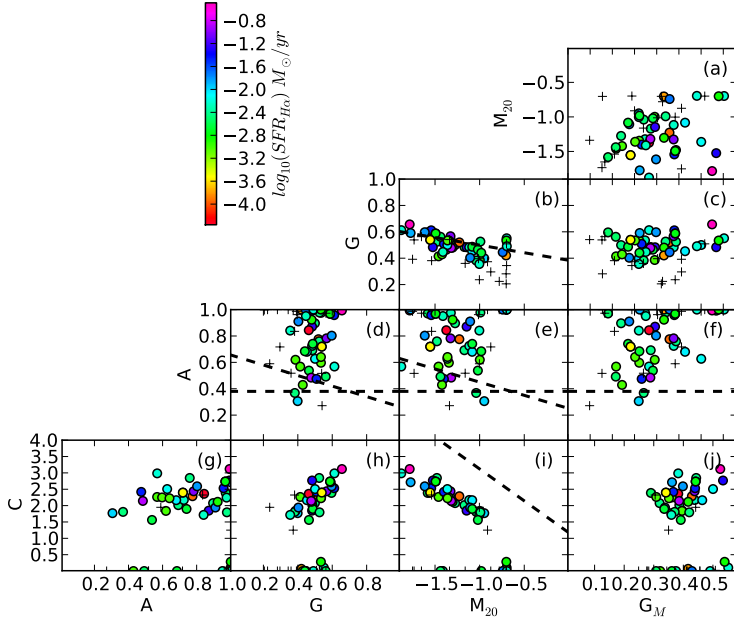


Figure 6. The distribution of the H I morphological parameters colour coded by the *total* star-formation rate inferred from H α flux from Hunter & Elmegreen (2004). None of the H I morphology parameter relate to the *total* star-formation, $\log_{10}(SFR) M_{\odot} \text{yr}^{-1}$ (Table 3).

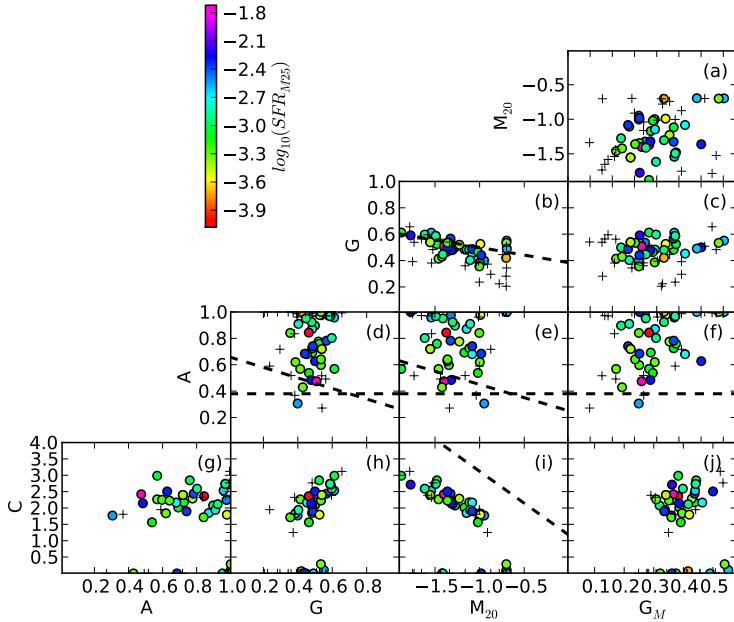


Figure 8. The distribution of the H I morphological parameters colour coded by the star-formation surface density over the optical disk (R_{25}), inferred from the H α flux, from Hunter & Elmegreen (2004). None of the H I morphology parameters are closely related to the H α surface brightness (Table 3).

where in H I morphology space, e.g., Figure 6, sub-panels (a), (g) or (j). However, a direct comparison between current star-formation and the H I morphology reveals little direct correlation between the H I morphology parameters and the current star-formation (Figure 5 and Table 3).

Figure 6 shows the distribution of H I column density map morphologies, coded by the star-formation sur-

face density ($\log_{10}(SFR_{M25})$) from Hunter & Elmegreen (2004), their Table 3, based on the H α luminosity over the 25 mag/arcsec² radius (R_{25}). A similar value can be obtained over the optical radius (R_D). The star-formation surface density stands out in H I morphology space in the Gini parameter (when computed over R_D , see Table 3).

Because the dwarfs straddle the Gini- M_{20} criterion for

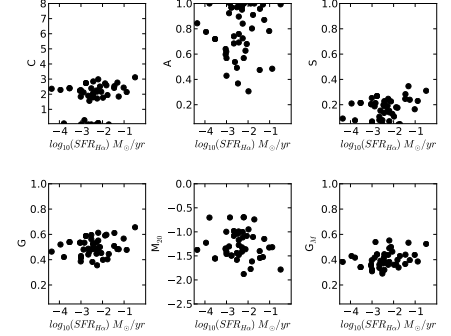


Figure 5. The relation between H α -derived SFR from Hunter et al. (2006) and the six morphology parameters.

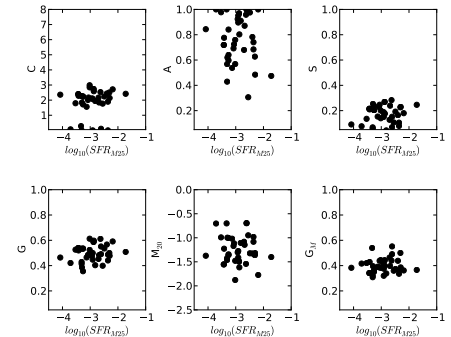


Figure 7. The star-formation surface density over the optical disk (R_{25}) from Hunter & Elmegreen (2004) compared to the H I morphology parameters. None of the H I morphology parameters are closely related to the H α surface brightness (Table 3).

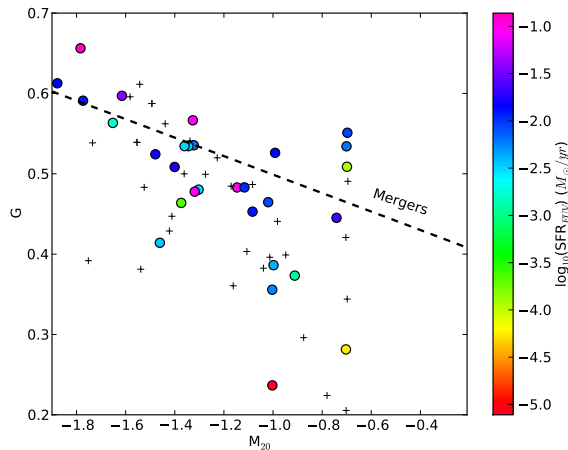


Figure 14. The M_{20} and Gini parameters of the H I maps colour coded by the star-formation rate based on FUV flux ($\log_{10}(SFR_{FUV})$) reported in Hunter et al. (2010). The dashed line is a criterion for major interaction from Holwerda et al. (2011a); Lotz et al. (2004).

interaction (equation 9), we explore these parameters with current star-formation surface density in detail in Figure 9. Lower star-formation surface densities ($\log_{10}(SFR_{M25}) < -3$) tend to lie below this interaction criterion while those above it have star-formation surface densities above it. That is not to say that those dwarfs are indeed interacting but their H I appearance parameterised by Gini- M_{20} combined and their current star-formation do appear to be linked.

4.2.2 Gas Exhaustion Time τ_c

Hunter & Elmegreen (2004) supply an estimate of the time it will take each galaxy to exhaust its gas supply (estimated from single-dish observations) by their current star-formation. Figure 11 shows the morphology distribution colour-coded by the gas exhaustion time (τ). The quickly exhausted galaxies are –unsurprisingly– those with a high star-formation surface density. The exhaustion time estimate is a simple one, otherwise one could perhaps expect a relation with the concentration of fuel or the Gini parameter (an indication of inequality). ISM in lumps close to the star-formation would be consumed much faster than a smooth gas disk that would need to coalesce in star-forming clouds first. However, the gas exhaustion time is not strongly related to any of the H I morphology parameters (Figure 10 and Table 3).

4.2.3 Recent Star-formation: SFR_{FUV}

Hunter et al. (2010) and McQuinn et al. *in prep* report FUV fluxes and derived star-formation rates. The McQuinn results are corrected for dust extinction using an estimate of the total far-infrared flux based on Spitzer/MIPS 24, 70 and 160 μm maps. The Hunter et al. values are not corrected for dust extinction. The general agreement between the Hunter et al. and McQuinn et al. values in a couple of overlap cases is good enough for us to combine both FUV star-formation

values sets to mark the points in Figure 13. In Figure 13, there are some weak trends already evident between recent star-formation (SFR_{FUV}) and the Gini and M_{20} values in H I, but no clear delineations in parameter-space. Figure 12 confirms these trends: Gini increases with SFR_{FUV} and M_{20} decreases, i.e., H I disks become less smooth (higher G) but relatively fewer bright spots at higher radii (lower M_{20}). The Spearman indices in Table 3 corroborate this and also reveal (weak) relations with Concentration and G_M with recent star-formation. Figure 14 highlights the Gini- M_{20} relation. The majority of galaxies with an SFR_{FUV} measurement straddle the G- M_{20} interaction line. To better constrain the relation between H I Gini and M_{20} (and other H I morphological parameters) the sample of SFR_{FUV} measurements will need to be expanded to include all VLA-ANGST and LITTLE-THINGS galaxies.

Hunter et al. (2010) also provide comparisons to the star-formation rates inferred from H α fluxes from Hunter & Elmegreen (2004) and a V-band photometry-based star-formation rate. These values could possibly provide a useful direct comparison to which time-scale of ongoing star-formation dominates the morphology for the same sample. The figures in Appendix B show the dependence of H I morphology on these ratios, $SFR_{FUV}/SFR_{H\alpha}$ and SFR_{FUV}/SFR_V in Figures B2 and B4 respectively. Apart from some suggestive clusterings of a few points, there is no real relation between the $SFR_{FUV}/SFR_{H\alpha}$ ratio and H I morphology. There may be a some relation between the SFR_{FUV}/SFR_V ratio and Gini (see Table 3).

4.3 Resolved stellar populations: Star-formation History

One of the main science drivers behind the ANGST survey was to obtain an accurate star-formation history from the resolved stellar population as observed with the Hubble Space Telescope (see Dalcanton et al. 2009; Weisz et al. 2011c,a,b, 2012a,b; McQuinn et al. 2010a,b, 2012a,b). The main values to compare to the H I morphology are the mean star-formation time, the mass-to-light ratio and the mean age of the stars in each galaxy from Weisz et al. (2011a), their Tables 2 and 3, supplemented with a few average star-formation rates $\langle SFR \rangle$ values from McQuinn et al. (2012b), their Table 1. Based on the (weak) relations with ongoing star-formation tracers in the previous sections, one could expect some correlation between the shape of the atomic hydrogen distribution and the star-formation history, depending on the typical time-scale of the relation.

Figure 16 shows the H I morphology, colour-coded for the ANGST sample by the average star-formation rate ($\langle SFR \rangle$) over the entire history of the galaxy, calculated over the past 10 Gyr (Weisz et al. 2011a) or 6 Gyr (McQuinn et al. 2012b). Figure 15 shows the direct relation between the typical star-formation over these longer time-scales $\langle SFR \rangle$ and the H I morphology parameters. Those galaxies with low star-formation rates are typically low in Gini, G_M , and Asymmetry, and high in M_{20} values. The G_M and M_{20} values appear to be related for those galaxies with a low lifetime star-formation rate ($\sim 10^{-3} M_{\odot}/\text{yr}$). The Spearman indices are high for M_{20} and Gini: $\langle SFR \rangle$ is anti-correlated to M_{20} , and correlated with Gini.

Thus, there is some relation between the mean star-

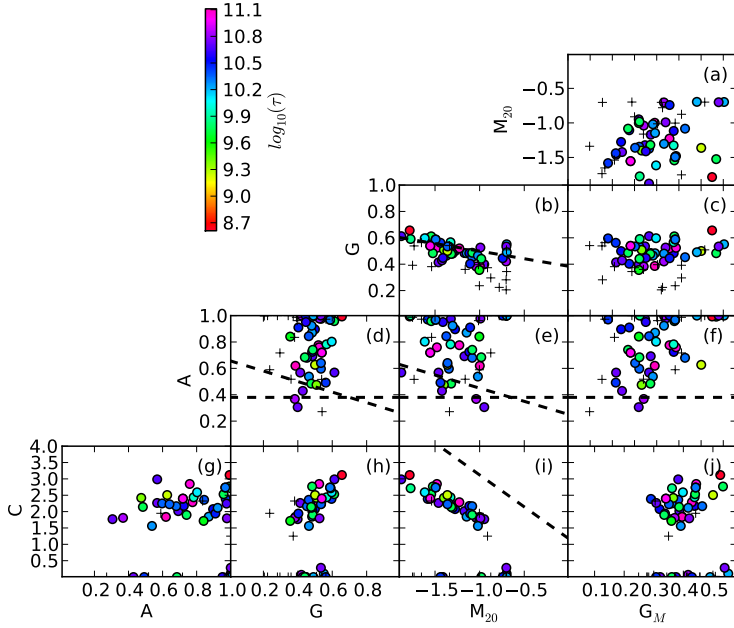


Figure 11. The distribution of the H I morphological parameters colour coded by the gas exhaustion time estimate from Hunter & Elmegreen (2004). Dashed lines are the criteria for major interaction from Holwerda et al. (2011a), based on the WHISP sample or established morphological selections of mergers in optical data. None of the H I morphological parameters are closely related to the exhaustion time (Table 3).

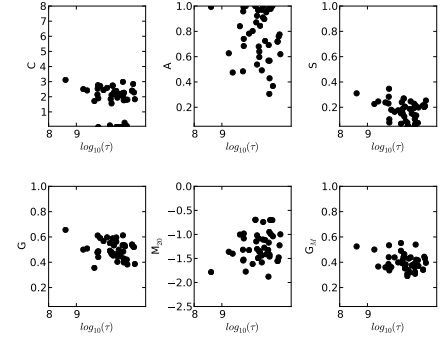


Figure 10. The relation between gas exhaustion time estimate from Hunter & Elmegreen (2004) and the H I morphological parameters. None of the H I morphological parameters are closely related to the exhaustion time (Table 3).

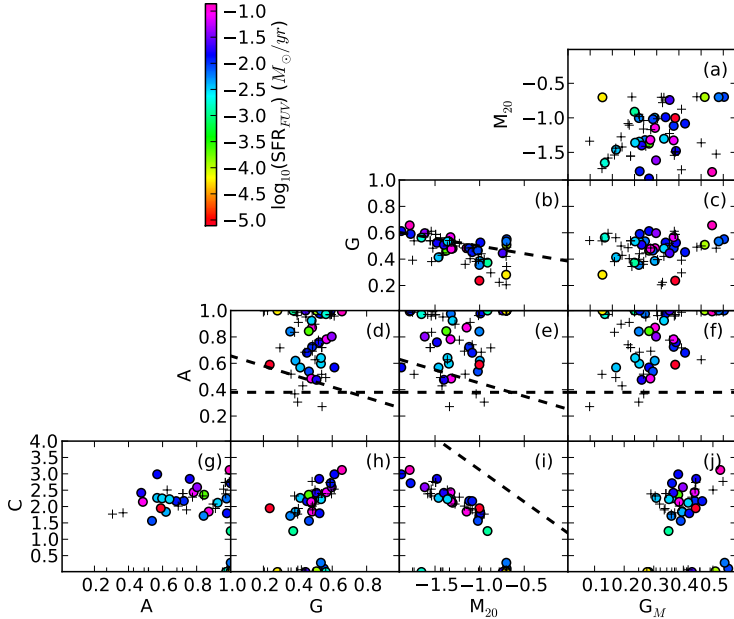


Figure 13. The distribution of the H I morphological parameters colour coded by the star-formation rate based on FUV flux ($\log_{10}(SFR_{FUV})$) reported in Hunter et al. (2010). Some weak trends visible between the SFR and the Gini and M_{20} values in H I, but without clear delineations. The Spearman indices in Table 3 point to a strong correlation with both Concentration and Gini, a weaker one with M_{20} and G_M .

formation rate in a dwarf galaxy and how the H I is distributed. Galaxies that are not forming stars at a high rate right now and have not in the past ($\langle SFR \rangle \sim 1 - 2 \times 10^{-3} M_{\odot}/yr$) show lower values of Gini, G_M and higher values of M_{20} .

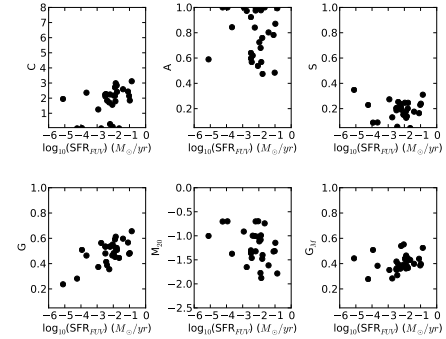


Figure 12. The relation between FUV-derived SFR from Hunter et al. (2010) and the six morphology parameters.

In comparison, appendix C shows that there is little or no relation with mass-to-light ratio or mean stellar age from Weisz et al. (2011a).

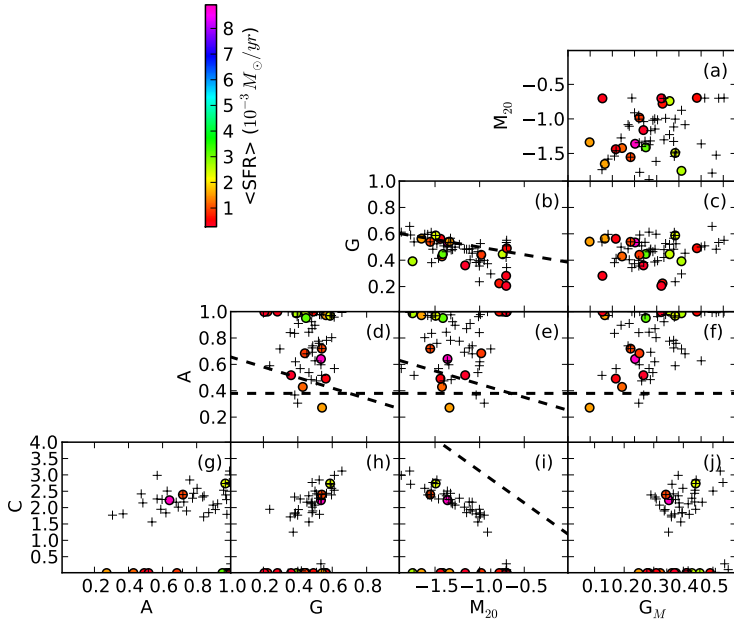


Figure 16. The morphology of the H I maps colour coded by the mean past star-formation rate from Weisz et al. (2011a) or McQuinn et al. (2012b). There are relatively strong anti-correlations with M_{20} and related to the Gini parameter.

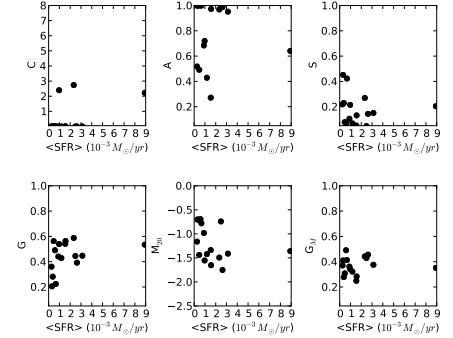


Figure 15. The relation between V -band derived SFR from Weisz et al. (2011a) and the six morphology parameters.

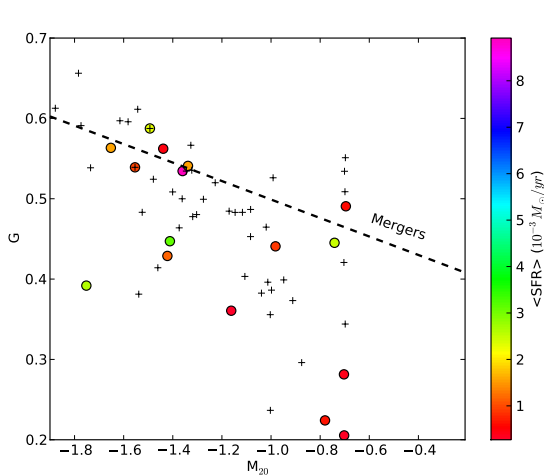


Figure 17. The M_{20} and Gini parameters of the H I maps colour coded by the mean past star-formation rate from Weisz et al. (2011a) or McQuinn et al. (2012b). The dashed line is a criterion for major interaction from Holwerda et al. (2011a); Lotz et al. (2004).

4.4 Extended H α disks

In Holwerda et al. (2012), we used these parameters to identify extended UV disks (XUV) in the *WHISP* survey. Hunter & Elmegreen (2004) note the relative scale of the H II regions to that of the optical disk (R_{25}), Holmberg radius (R_H), and disk scale length (R_D). Figure 18 shows the morphological parameters distribution, colour coded by the relative extent of the H α emission. The highest correlation between these axes ratios with the H I parameters is with M_{20} and anti-correlated with Gini (Table 3).

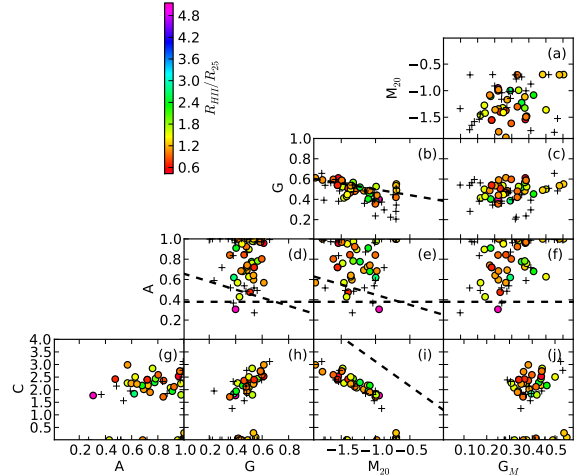


Figure 18. The distribution of the H I morphological parameters colour coded by the relative extent of the H α disk (R_{HII}/R_{25}) from Hunter & Elmegreen (2004). Dashed lines are the criteria for major interaction from Holwerda et al. (2011a), based on the *WHISP* sample or established morphological selections of mergers in optical data. The ratio is related with the M_{20} and anti-correlated to the Gini parameter (Table 3), already identified in Holwerda et al. (2012) as the right combination to identify extended star-formation disks.

We find that galaxies that have a high star-formation surface density, are also relatively compact. Figure 19 shows the Asymmetry- M_{20} for the H I maps and the XUV disk criterion for 6" FUV data from Holwerda et al. (2012). Eleven galaxies are in this selection. Five have extended H II radii ($R_{HII}/R_{25} > 1$), and five of these do not have a H II radius from Hunter & Elmegreen (2004) (Figure 18). The one

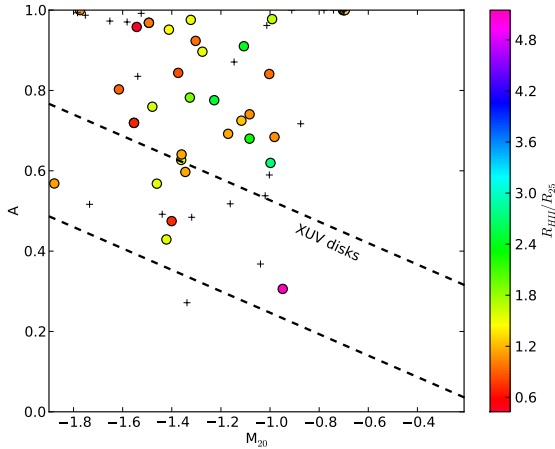


Figure 19. The Asymmetry and M_{20} of the H I maps colour coded by the relative extent of the H α disk ($R_{H\alpha}/R_D$) from Hunter & Elmegreen (2004). The dashed lines are the XUV disk criteria identified in Holwerda et al. (2012) for FUV images.

R_{HII}/R_{25} extreme value in our sample is selected but the remainder is not exceptionally extended or concentrated. We conclude that extended HII disks are not related to extended FUV disks.

5 THE STAR-FORMATION AND H I MORPHOLOGY RELATIONS SPIRALS AND IRREGULARS

In the past few sections, we have tried to establish if there is a relation between the quantified H I morphological parameters of dwarf galaxies and their star-formation measured over different time-scales by different tracers. To place this in a larger context, we will now compare the quantified H I morphology parameters of *all* our samples, THINGS (Holwerda et al. 2011c), WHISP (Holwerda et al. 2011d), LITTLE-THINGS and VLA-ANGST (this paper) to a common star-formation and stellar mass estimate from the Sloan Digital Sky Survey from Brinchmann et al. (2004).

Total stellar mass, total star-formation and specific star formation are available for the SDSS DR7 sample of galaxies as described by Kauffmann et al. (2003) and Brinchmann et al. (2004) here: <http://www.mpa-garching.mpg.de/SDSS/DR7/>. Cross-correlating with position, we obtain a common measurements for our full H I sample. We note that these measures are based on a 3'' aperture typically centered on the galaxy nucleus.

The H I samples divides into two sub-samples: a high spatial resolution ($\sim 6''$), the VLA-ANGST and THINGS surveys, and a lower resolution one (~ 10 - $12''$), the WHISP and LITTLE-THINGS surveys. We will do the comparison with the SDSS parameters for the combined and the high- and low-resolution subsamples. To distinguish these plots from the previous comparisons, the markers are triangles for the low-resolution sample and squares for the high-resolution sample in the following plots.

We note two caveats in the comparison: first, the inter-

ferometric observations miss low-intensity, large-scale emission (see section 3.1). This introduces a different sensitivity in the low and high-resolution maps to diffuse, large-scale tidal features for example. And secondly, the SDSS survey skipped very nearby galaxies which were resolved in individual HII regions for spectroscopic follow-up (e.g., M101 is not in the SDSS DR7 spectroscopic sample).

5.1 Stellar Mass

The range in stellar masses is lower than one would expect (Figure 21), given that two of the surveys target dwarf systems (VLA-ANGST and LITTLE-THINGS) but many of these galaxies do not feature in the SDSS DR7 spectroscopic catalog. Figure 20 shows the relation (if any) between the six H I morphological parameters and the stellar mass ($\log_{10}(M_*/M_\odot)$). There appears to be little or no relation between a galaxy's stellar mass and the H I morphology, in the full or either the high or lower-resolution samples (6'' and 12'' respectively, see Table 4).

5.2 Star-Formation

Figure 23 shows the distribution of H I morphology parameters but now colour-coded by total star-formation ($\log(SFR)$). There are a few suggestive outliers, especially with respect to the Gini parameters (panel (b)), but a clean trend is impossible to distinguish. In the plot of star-formation rate against the six H I morphology parameters in Figure 22, clear trends are also absent, as reflected in the spearman rankings for the full sample (Table 4). However, there is an interesting difference between the low- and high-resolution samples: in there a much better correlations between the overall H I morphology and the total star-formation in the high-resolution sample (6'').

In the high-resolution sample, star-formation is weakly related to Asymmetric, Smoothness, M_{20} , Gini, and G_M . This is similar to what we found for the smaller systems (Table 3), but some of the relations are inverted (e.g., SFR and Gini). The inversion of the relation between star-formation and those H I parameters that measure the clumpiness of the ISM is intriguing: if one extends the mass range of the sample to high-mass galaxies (in fact the high-resolution sample is dominated by them), the Gini parameters *lowers* slightly with higher star-formation (Figure 22, and more clearly in Table 4). One could speculate that in high-mass, high-star-formation cases, the clumping is taken to extremes and the majority of hydrogen is in dense molecular clumps, leaving a relatively smooth H I disk.

Because many of the dwarf systems do not have a reliable H α star-formation traces in SDSS, primarily because their stellar light is too diffuse, we plot the combination of the Hunter et al. (2006) values and the Brinchmann et al. (2004) values in Figure 26 for Gini, G_M and M_{20} . We note that there is some relation, but most interestingly the range of H I morphology values increases to higher star-formation (and the higher-mass systems).

Table 3. The Spearman correlation between various literature values and the HI morphological parameters. Ranking is only computed for where both the literature values and HI morphological values are available. Notable rankings are marked in bold; these are parameters between which there is a (weak) linear relation. Positive values indicate correlation, negative ones anti-correlation.

Name	C	A	S	M_{20}	G	G_M	note
v_{rot}	0.23	-0.06	-0.04	-0.02	0.05	0.33	
from Karachentsev et al. (2004):							
Θ	-0.03	0.42	-0.02	0.14	-0.03	0.21	(1)
from Hunter et al. (2006):							
M_{HI}/L	-0.13	-0.13	-0.46	-0.11	0.00	-0.25	(2)
$\log_{10}(SFR)M_{\odot}/yr$	0.17	0.15	0.16	-0.06	0.13	0.32	(3)
$\log_{10}(SFR_{M25})$	0.12	-0.01	0.06	0.00	0.16	0.12	(4)
$\log_{10}(SFR_D)$	0.32	0.17	0.23	-0.24	0.44	0.28	(5)
$\log_{10}(\tau)$	-0.20	-0.14	-0.23	0.13	-0.21	-0.22	(6)
R_{HII}/R_{25}	-0.28	-0.17	-0.33	0.40	-0.36	0.07	(7)
R_{HII}/R_H	-0.29	-0.11	-0.21	0.61	-0.40	0.23	(8)
R_{HII}/R_D	-0.09	-0.17	-0.15	0.34	-0.10	0.23	(9)
from Weisz et al. (2011a) and McQuinn et al. (2012a):							
f_{10}	-0.14	-0.26	-0.19	0.05	-0.16	0.25	
f_{06}	0.03	-0.21	-0.14	-0.16	0.16	-0.02	
f_{03}	-0.26	0.15	0.41	0.14	-0.30	0.01	
f_{02}	-0.28	0.28	0.48	0.27	-0.42	-0.13	
f_{01}	-0.07	-0.01	0.38	0.07	-0.12	-0.29	
Mean Stellar Age (Gyr)	-0.07	-0.26	-0.09	-0.02	-0.10	0.20	(10)
$\langle SFR \rangle (10^{-3}M_{\odot}/yr)$	0.35	-0.08	-0.30	-0.50	0.44	0.15	(11)
Mass-to-light ratio	-0.11	0.08	-0.11	0.11	-0.07	0.05	(12)
from Hunter et al. (2010) and McQuinn et al. <i>in preparation</i> :							
$\log_{10}(SFR_{FUV}) (M_{\odot}/yr)$	0.44	-0.14	0.03	-0.32	0.44	0.36	(13)
$\log_{10}(SFR_{H\alpha}) (M_{\odot}/yr)$	0.24	0.20	0.19	-0.20	0.48	0.21	(14)
$\log_{10}(SFR_V) (M_{\odot}/yr)$	0.38	-0.24	0.05	-0.38	0.32	0.06	(15)
$\log_{10}(SFR_{FUV}/SFR_{H\alpha}) (M_{\odot}/yr)$	0.15	-0.38	0.18	-0.15	-0.21	-0.04	(16)
$\log_{10}(SFR_{FUV}/SFR_V) (M_{\odot}/yr)$	-0.43	0.06	0.06	0.40	-0.53	-0.14	(17)
Mass-to-light $M/L_V (M_{\odot}/L_{\odot})$	-0.01	-0.25	-0.04	0.04	-0.22	-0.18	(18)

¹ Tidal parameter from Karachentsev et al. (2004).

² The mass-to-light ratio inferred in Hunter et al. (2006) from H α emission.

³ The *total* star-formation rate inferred in Hunter et al. (2006) from H α emission.

⁴ The star-formation rate over the R_{25} radius inferred in Hunter et al. (2006) from H α emission.

⁵ The star-formation rate over the R_D radius inferred in Hunter et al. (2006) from H α emission.

⁶ The gas-depletion time inferred by Hunter et al. (2006) from H α emission.

⁷ The ratio between the radius containing the HII regions to the de Vaucouleur radius R_{25} .

⁸ The ratio between the radius containing the HII regions to the Holmberg radius (R_H).

⁹ The ratio between the radius containing the HII regions to the optical radius (R_D).

¹⁰ The mean age of the stellar population computed from the fractions ($f_1 - f_{10}$) reported in Weisz et al. (2011a).

¹¹ The mean star-formation rate over the last 10 Gyr reported in Weisz et al. (2011a).

¹² The mean stellar mass-to-light ratio inferred from the stellar population in Weisz et al. (2011a).

¹³ The star-formation rate inferred from FUV flux reported in Hunter et al. (2010).

¹⁴ The star-formation rate inferred from H α flux reported in Hunter et al. (2010).

¹⁵ The star-formation rate inferred from V-band flux reported in Hunter et al. (2010).

¹⁶ The ratio between star-formation rates inferred from FUV and H α flux reported in Hunter et al. (2010).

¹⁷ The ratio between star-formation rates inferred from FUV and V-band flux reported in Hunter et al. (2010).

¹⁸ The inferred stellar mass-to-light ratio report reported in Hunter et al. (2010).

5.3 Specific Star-Formation

Normalizing the total star-formation with the stellar mass, there is again little or no relation between the HI morphology and the specific star-formation (Figures 25 and 24 and

table 4), either for the total or high- or low-resolution samples.

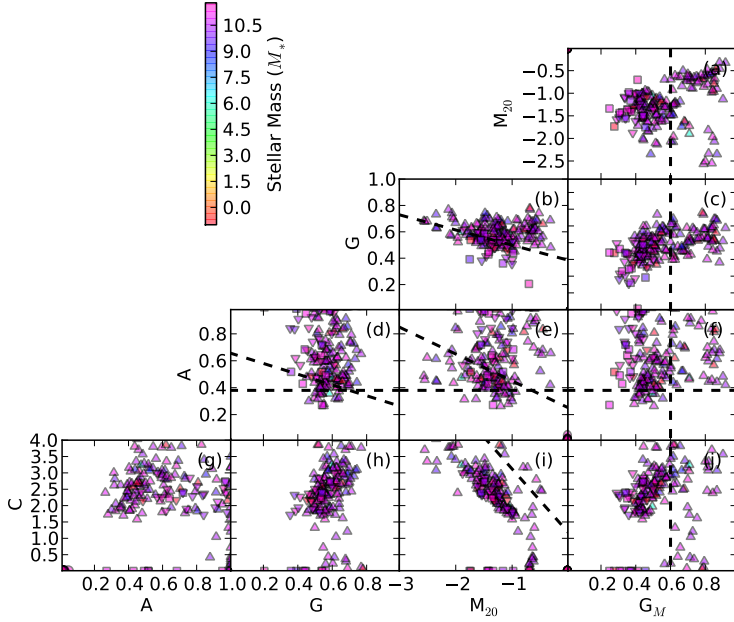


Figure 21. The distribution of H I morphologies for the full sample, colour-coded by their inferred stellar mass from Brinchmann et al. (2004), updated to the SDSS DR7.

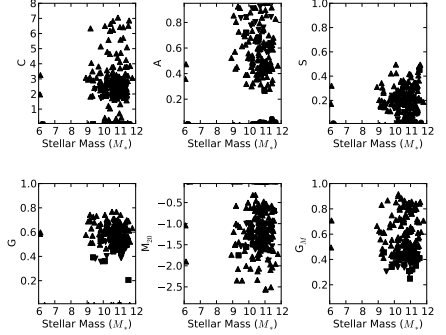


Figure 20. The direct relation between H I morphologies and their inferred stellar mass from Brinchmann et al. (2004), updated to the SDSS DR7.

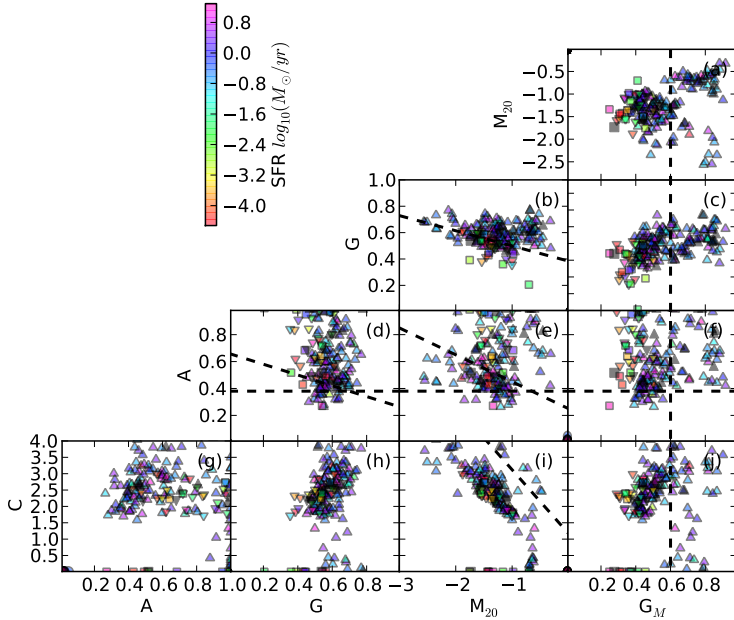


Figure 23. The distribution of H I morphologies for the full sample, colour-coded by their inferred total star-formation from Brinchmann et al. (2004), updated to the SDSS DR7.

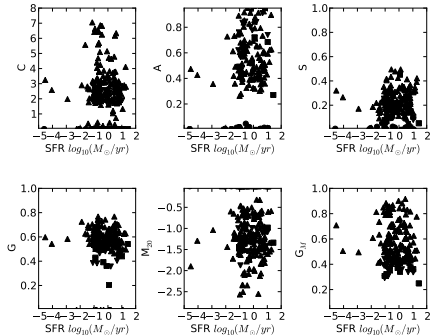


Figure 22. The direct relation between H I morphologies and their inferred total star-formation from Brinchmann et al. (2004), updated to the SDSS DR7.

6 DISCUSSION

As part of the local volume of galaxies, many dwarf galaxies can be expected to be tidally disrupted by either a close dwarf companion or a nearby massive galaxy (the Milky Way, Andromeda or M81). However, the H I morphology does not seem to be affected as much by tidal interaction as by star formation. Since these galaxies are relatively shallow gravitational potentials, one would expect the tidal forces to

play a significant role in the general shape of the ISM. However, the short kinematic time scales of the ISM may result in a quick relaxation of any tidal disturbance or tidal effects on the H I in these galaxies are too subtle to detect in this parameter space.

We compared the H I morphology to a series of star-formation indicators, sensitive to different time-scales of star-formation. The measures of inequality in the H I morphology, the Gini, G_M and M_{20} parameter are weakly re-

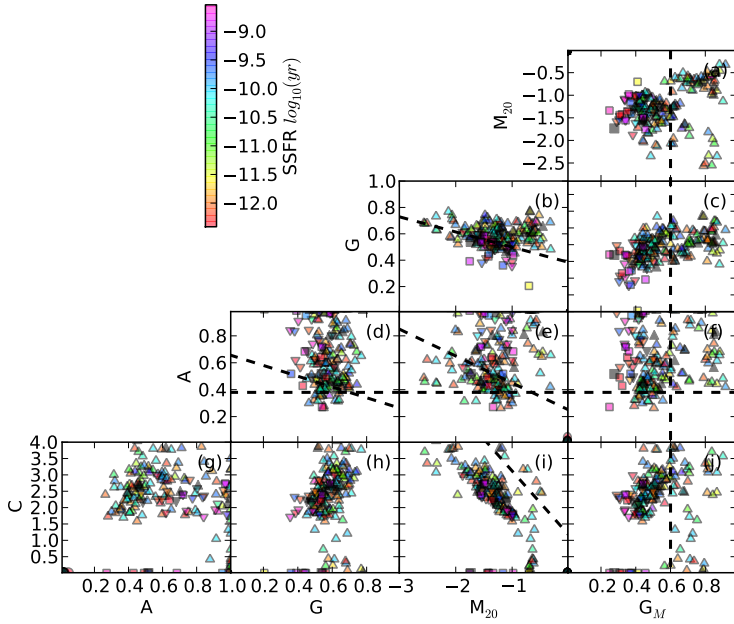


Figure 25. The distribution of H I morphologies for the full sample, colour-coded by their inferred specific star-formation from Brinchmann et al. (2004), updated to the SDSS DR7.

Table 4. The Spearman rank correlation of the H I morphological parameters with stellar mass, total, and specific star-formation of the high- (6''), low-resolution (12'') and full samples. There is very little relation between the H I morphology and star-formation for data at 12'' resolution. Star-formation's effects are more noticeable only in the high-resolution sample.

Sample & parameter	C	A	S	M_{20}	G	G_M
6''						
Star Formation Rate (SFR)	-0.05	0.44	0.34	-0.35	-0.36	0.36
Specific Star Formation Rate (SSFR)	-0.08	-0.07	-0.13	-0.17	-0.05	0.23
Stellar Mass (M_*)	-0.03	0.28	0.13	0.13	-0.08	-0.03
12''						
Star Formation Rate (SFR)	-0.04	0.01	0.15	-0.05	-0.07	-0.02
Specific Star Formation Rate (SSFR)	-0.05	-0.02	0.04	-0.03	-0.01	-0.04
Stellar Mass (M_*)	-0.01	-0.01	0.00	-0.03	-0.04	-0.01
All						
Star Formation Rate (SFR)	0.00	0.08	0.17	-0.10	-0.13	0.02
Specific Star Formation Rate (SSFR)	-0.05	-0.00	0.02	-0.04	-0.02	-0.03
Stellar Mass (M_*)	-0.01	-0.00	0.01	-0.01	-0.05	-0.01

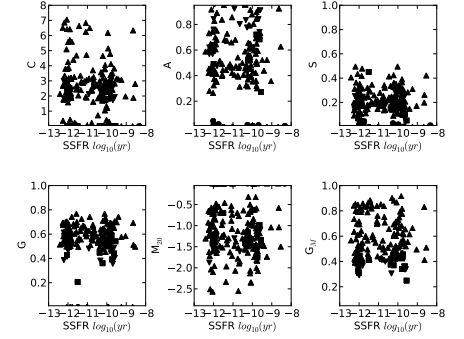


Figure 24. The direct relation between H I morphologies and their inferred specific star-formation from Brinchmann et al. (2004), updated to the SDSS DR7.

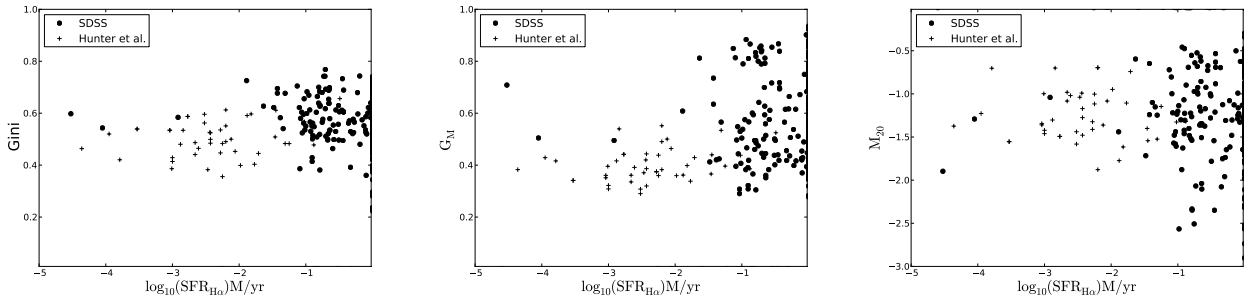


Figure 26. The relation between star-formation from H α and the Gini, G_M and M_{20} parameters. Crosses are the morphologies of the LITTLE-THINGS galaxies with H α star-formation from Hunter et al. (2006) and the dots are the other surveys with star-formation from Brinchmann et al. (2004), based on the SDSS spectra. There is a weak relation with both Gini and G_M . We note that the spread in all three values goes up with star-formation.

lated to various tracers of star-formation ($H\alpha$, FUV or based on resolved stellar population). This result is largely in line with what is becoming the general picture of these galaxies: the local physics dominate over environment (McQuinn et al. 2012a).

That is not to say that the star-formation is the shaping agent of the H I morphology through, for example, supernova feedback and stellar winds. The reverse could well be true; the inequality distributed ISM more often generates the conditions for local star-formation. McQuinn et al. (2012a) show that the star-formation is stochastic both in time and location within star-bursting galaxies, corroborating such a scenario. And interestingly, the *mean* star-formation rate of the galaxies appear to be related to the H I morphological parameters as well as the current star-formation indicator (Figure 6). We propose a scenario where as soon as the ISM is transformed to an unequal or clumpy state, most likely by an external trigger –e.g., tidal or gravitational turbulence from the inflow of gas– the star-formation rate is elevated. The combined effect of elevated star-formation and the external factor keep the ISM clumpy over longer time-scales than the current (ionizing, $H\alpha$) star-formation timescale.

We note a few things in the comparison of *all* the H I morphological parameters available and a common stellar mass and star-formation estimates from SDSS (section 5). First, any relation manifests itself only in the *high-resolution* ($\sim 6''$) sample and not in the lower-resolution one. Because the sampling is sub-kpc typically in the high-resolution sample, this scale is one where the effects of feedback from star-formation (or the effect of H I overdensities on star-formation) can be seen. Coarser observations simply wash any ISM-star-formation relation out.

The importance of sampling on our study of the effects of star-formation on the ISM is noteworthy for the future all-sky H I surveys (the WNSHS survey with the WSRT/APERTIF and the Wallaby survey with ASKAP, Koribalski et al. *in preparation*). The spatial resolution of these surveys is expected to be $\sim 10''$, which means that the effects of star-formation on the H I morphology will largely be smoothed out. While these surveys will be indispensable to identify exceptional systems and characterize global gas characteristics in disks, follow-up observations at higher resolution will remain essential to characterize the interplay of star-formation and the ISM.

Secondly, the effects of star-formation reversed for some parameters when we compared for a low-mass sample (LITTLE-THINGS and VLA-ANGST) to the high-resolution sample (VLA-ANGST and THINGS). For example, the relation between total star-formation and the Gini parameter (or M_{20} or G_M) reverses sign (Tables 4 and 3). We put forward that in low-mass systems, it is predominantly the H I that is related and regulates the star-formation (as argued by Bigiel et al. 2008) but in a higher-mass sample, the molecular component is the dominant ISM component in the relation with star-formation. That is to say, the clumping seen in the H I of low-mass systems with increased star-formation happens in the molecular phase in more massive systems, leaving a relatively smooth H I disk. Therefore the Gini parameter lowers with star-formation if one includes more massive galaxies.

And the third point to make is that Asymmetry is strongly related to star-formation for the high-resolution

subsample. This could be indirect evidence of gas accretion, especially for massive systems, as a strong relation between any of the star-formation tracers and H I Asymmetry is absent in the low-mass sample (Table 3). The relation between Asymmetry and M_{20} for XUV disks reported in Holwerda et al. (2012) certainly appears to hint in that direction. However, this could also be taken as evidence of star-formation feedback on larger scales. Fact remains that the strongest and most consistent relationship in the high-resolution sample is between star-formation and H I Asymmetry.

7 CONCLUSION

We applied the quantified morphology parameterization to two H I surveys of nearby dwarf galaxies, LITTLE-THINGS and VLA-ANGST, and compared these to indicators of interaction and star-formation. We find that:

(i) The H I morphological criteria for interaction, developed for use on massive galaxies do not apply to these smaller dwarf irregular galaxies (Figure 4).

(ii) A low value of the Asymmetry of the H I map may point to an isolated dwarf (Figure 4).

(iii) Current star-formation surface density ($H\alpha$) is related to the H I morphology, specifically the Gini, G_M , and M_{20} parameters. These indicate a stronger inequality in the neutral ISM distribution (Figure 8 & 6).

(iv) Consequently, clumpy H I is also the quickest depleted (Figure 11).

(v) Based on previous resolved stellar population results, the star-formation (current and history) is linked to the Gini, G_M , and M_{20} parameters of the H I maps (Figure 16): high star-formation and unequally distributed H I are closely linked but not necessarily causal.

(vi) Over a large sample of galaxies, spanning a wider mass range, there is no relation between stellar mass, total or specific star-formation (Table 4 and Figures 21, 20, 23, 22, 25, and 24).

(vii) To detect any relation between star-formation tracers and H I morphology, high-resolution ($\sim 6''$) H I maps are critical (Table 4).

(viii) There is a relation between H I Asymmetry and the ongoing *total* star-formation in massive galaxies (Figure 22, Table 4).

Future applications of the quantified morphology parameters on H I maps will be on the large catalogs of moderately resolved galaxies in the WNSHS (Jozsa et al. *in preparation*) and WALLABY (Koribalski et al. *in preparation*) surveys. These will produce significantly improved statistics on H I morphology which can then be combined with all-sky surveys of star-formation tracers (e.g., GALEX and WISE catalogs).

ACKNOWLEDGEMENTS

The authors would like to thank the anonymous referee whose comments and suggestions improved the manuscript significantly. The lead author thanks Dr McQuinn for the useful discussions on the topic of dwarfs and their star-formation and for making her FUV star-formation estimates

available to us and A. Leroy for the suggestion for the comparison against SDSS measures. The authors thank C. Carignan for making the H I moment-0 map of NGC 3109 from the Karoo Array Telescope available for a direct comparison with VLA data.

The lead author thanks the European Space Agency for the support of the Research Fellowship program. We thank the National Radio Astronomy Observatory for their generous time allocation, observing, and data reduction support for these two Large Projects, the LITTLE-THINGS and VLA-ANGST. The National Radio Astronomy Observatory is a facility of the National Science Foundation operated under cooperative agreement by Associated Universities, Inc. We would like to thank the LITTLE-THINGS and VLA-ANGST teams for their effort on the calibration and imaging and making their products available to the astronomical community. This research has made use of the NASA/IPAC Extragalactic Database (NED) which is operated by the Jet Propulsion Laboratory, California Institute of Technology, under contract with the National Aeronautics and Space Administration. This research has made use of NASA's Astrophysics Data System.

REFERENCES

- Berg D. A., Skillman E. D., Marble A. R., van Zee L., Engelbracht C. W., Lee J. C., Kennicutt Jr. R. C., Calzetti D., Dale D. A., Johnson B. D., 2012, *ApJ*, 754, 98
- Bertin E., Arnouts S., 1996, *A&AS*, 117, 393, provided by the NASA Astrophysics Data System
- Bigiel F., Leroy A., Walter F., Brinks E., de Blok W. J. G., Madore B., Thornley M. D., 2008, *AJ*, 136, 2846
- Booth R. S., de Blok W. J. G., Jonas J. L., Fanaroff B., 2009, *ArXiv e-prints/0910.2935*
- Bouché N., Lehnert M. D., Aguirre A., Péroux C., Bergeron J., 2007, *MNRAS*, 378, 525
- Brinchmann J., Charlot S., White S. D. M., Tremonti C., Kauffmann G., Heckman T., Brinkmann J., 2004, *MNRAS*, 351, 1151
- Cannon J. M., Giovanelli R., Haynes M. P., Janowiecki S., Parker A., Salzer J. J., Adams E. A. K., Engstrom E., Huang S., McQuinn K. B. W., Ott J., Saintonge A., Skillman E. D., Allan J., Erny G., Fliss P., Smith A., 2011, *ArXiv e-prints*
- Carignan C., Frank B. S., Hess K. M., Lucero D. M., Randraimampandry T. H., Goedhart S., Passmoor S. S., 2013, *ArXiv e-prints*
- Conselice C. J., 2003, *ApJS*, 147, 1
- Dalcanton J., Williams B., Gogarten S., Weisz D., Skillman E., Seth A., ANGST Team, 2007, in *American Astronomical Society Meeting Abstracts*, Vol. 211, *American Astronomical Society Meeting Abstracts*, pp. 79.05–+
- Dalcanton J. J., Williams B. F., Seth A. C., Dolphin A., Holtzman J., Rosema K., Skillman E. D., Cole A., Girardi L., Gogarten S. M., Karachentsev I. D., Olsen K., Weisz D., Christensen C., Freeman K., Gilbert K., Gallart C., Harris J., Hodge P., de Jong R. S., Karachentseva V., Mateo M., Stetson P. B., Tavarez M., Zaritsky D., Governato F., Quinn T., 2009, *ApJS*, 183, 67
- de Blok W. J. G., Jonas J., Fanaroff B., Holwerda B. W., Bouchard A., Blyth S., van der Heyden K., Pirzkal N., 2009, in *Panoramic Radio Astronomy: Wide-field 1-2 GHz Research on Galaxy Evolution*
- Domingue D. L., Keel W. C., White III R. E., 2000, *ApJ*, 545, 171
- Geha M., Blanton M., Yan R., Tinker J., 2012, *ArXiv e-prints*
- Grcevich J., Putman M. E., 2009, *ApJ*, 696, 385
- Holwerda B. W., 2005, *astro-ph/0512139*
- Holwerda B. W., Böker T., Dalcanton J. J., Keel W. C., de Jong R. S., 2013, *MNRAS*
- Holwerda B. W., de Blok W. J. G., Bouchard A., Blyth S., van der Heyden K., Pirzkal N., 2009, in *Conference Proceedings of the "Panoramic Radio Astronomy: Wide-field 1-2 GHz research on galaxy evolution"*, June 02 - 05, 2009 Groningen, the Netherlands
- Holwerda B. W., Keel W. C., 2013, *ArXiv e-prints*
- Holwerda B. W., Keel W. C., Bolton A., 2007, *AJ*, 134, 2385
- Holwerda B. W., Pirzkal N., Cox T. J., de Blok W. J. G., Weniger J., Bouchard A., Blyth S.-L., van der Heyden K. J., 2011a, *MNRAS*, 416, 2426
- Holwerda B. W., Pirzkal N., de Blok W. J. G., Bouchard A., Blyth S.-L., van der Heyden K. J., 2011b, *MNRAS*, 416, 2437
- Holwerda B. W., Pirzkal N., de Blok W. J. G., Bouchard A., Blyth S.-L., van der Heyden K. J., Elson E. C., 2011c, *MNRAS*, 416, 2401
- , 2011d, *MNRAS*, 416, 2415
- Holwerda B. W., Pirzkal N., de Blok W. J. G., van Driel W., 2011e, *MNRAS*, 416, 2447
- Holwerda B. W., Pirzkal N., Heiner J. S., 2012, *MNRAS*, 427, 3159
- Hunter D. A., Elmegreen B. G., 2004, *AJ*, 128, 2170
- , 2006, *ApJS*, 162, 49
- Hunter D. A., Elmegreen B. G., Ludka B. C., 2010, *AJ*, 139, 447
- Hunter D. A., Elmegreen B. G., Martin E., 2006, *ArXiv Astrophysics e-prints*
- Hunter D. A., Ficut-Vicas D., Ashley T., Brinks E., Cigan P., Elmegreen B. G., Heesen V., Herrmann K. A., Johnson M., Se-Heon, Rupen M. P., Schrubba A., Simpson C. E., Walter F., Westpfahl D. J., Young L. M., Zhang H.-X., 2012, *ArXiv e-prints*
- Jonas J., 2007, in *From Planets to Dark Energy: the Modern Radio Universe*. October 1-5 2007, The University of Manchester, UK. Published online at SISSA, *Proceedings of Science*, p.7
- Karachentsev I. D., Karachentseva V. E., Huchtmeier W. K., Makarov D. I., 2004, *AJ*, 127, 2031
- Kauffmann G., Heckman T. M., White S. D. M., Charlot S., Tremonti C., Brinchmann J., Bruzual G., Peng E. W., Seibert M., Bernardi M., Blanton M., Brinkmann J., Castander F., Csábai I., Fukugita M., Ivezić Z., Munn J. A., Nichol R. C., Padmanabhan N., Thakar A. R., Weinberg D. H., York D., 2003, *MNRAS*, 341, 33
- Keel W. C., Manning A. M., Holwerda B. W., Mezzoprete M., Lintott C. J., Schawinski K., Gay P., Masters K. L., 2013, *PASP*, 125, 2
- Keel W. C., White III R. E., 2001a, *AJ*, 121, 1442
- , 2001b, *AJ*, 122, 1369
- Kirby E. N., Martin C. L., Finlator K., 2011, *ApJ*, 742, L25

- Lotz J. M., Jonsson P., Cox T. J., Croton D., Primack J. R., Somerville R. S., Stewart K., 2011, *ApJ*, 742, 103
- Lotz J. M., Jonsson P., Cox T. J., Primack J. R., 2010a, *MNRAS*, 404, 590
- , 2010b, *MNRAS*, 404, 575
- Lotz J. M., Primack J., Madau P., 2004, *AJ*, 128, 163
- McQuinn K. B. W., Skillman E. D., Cannon J. M., Dalcanton J., Dolphin A., Hidalgo-Rodríguez S., Holtzman J., Stark D., Weisz D., Williams B., 2010a, *ApJ*, 721, 297
- , 2010b, *ApJ*, 724, 49
- McQuinn K. B. W., Skillman E. D., Cannon J. M., Dalcanton J. J., Dolphin A., Stark D., Weisz D., 2009, *ApJ*, 695, 561
- McQuinn K. B. W., Skillman E. D., Dalcanton J. J., Cannon J. M., Dolphin A. E., Holtzman J., Weisz D. R., Williams B. F., 2012a, *ArXiv e-prints*
- McQuinn K. B. W., Skillman E. D., Dalcanton J. J., Dolphin A. E., Cannon J. M., Holtzman J., Weisz D. R., Williams B. F., 2012b, *ApJ*, 751, 127
- Oh S.-H., de Blok W. J. G., Brinks E., Walter F., Kennicutt Jr. R. C., 2011, *AJ*, 141, 193
- Ott J., Stilp A. M., Warren S. R., Skillman E. D., Dalcanton J. J., Walter F., de Blok W. J. G., Koribalski B., West A. A., 2012, *ArXiv e-prints*
- Scarlata C., Carollo C. M., Lilly S., Sargent M. T., Feldmann R., Kampczyk P., Porciani C., Koekemoer A., Scoville N., Kneib J.-P., Leauthaud A., Massey R., Rhodes J., Tasca L., Capak P., Maier C., McCracken H. J., Mobasher B., Renzini A., Taniguchi Y., Thompson D., Sheth K., Ajiki M., Aussel H., Murayama T., Sanders D. B., Sasaki S., Shioya Y., Takahashi M., 2007, *ApJS*, 172, 406
- Skillman E., 2010, in *JENAM 2010, Joint European and National Astronomy Meeting*
- Skillman E. D., Simones J., Weisz D. R., Dalcanton J. J., Williams B. F., PHAT team, 2012, in *American Astronomical Society Meeting Abstracts, Vol. 219, American Astronomical Society Meeting Abstracts*, p. #151.07
- Swaters R. A., Sancisi R., van Albada T. S., van der Hulst J. M., 2011, *ArXiv e-prints*
- Tremonti C. A., Heckman T. M., Kauffmann G., Brinchmann J., Charlot S., White S. D. M., Seibert M., Peng E. W., Schlegel D. J., Uomoto A., Fukugita M., Brinkmann J., 2004, *ApJ*, 613, 898
- Walter F., Brinks E., de Blok W. J. G., Bigiel F., Kennicutt R. C., Thornley M. D., Leroy A., 2008, *AJ*, 136, 2563
- Warren S. R., Skillman E. D., Stilp A. M., Dalcanton J. J., Ott J., Walter F., Petersen E. A., Koribalski B., West A. A., 2012, *ArXiv e-prints*
- Weisz D. R., Dalcanton J. J., Williams B. F., Gilbert K. M., Skillman E. D., Seth A. C., Dolphin A. E., McQuinn K. B. W., Gogarten S. M., Holtzman J., Rosema K., Cole A., Karachentsev I. D., Zaritsky D., 2011a, *ApJ*, 739, 5
- Weisz D. R., Dolphin A. E., Dalcanton J. J., Skillman E. D., Holtzman J., Williams B. F., Gilbert K. M., Seth A. C., Cole A., Gogarten S. M., Rosema K., Karachentsev I. D., McQuinn K. B. W., Zaritsky D., 2011b, *ApJ*, 743, 8
- Weisz D. R., Johnson B. D., Johnson L. C., Skillman E. D., Lee J. C., Kennicutt R. C., Calzetti D., van Zee L., Bothwell M., Dalcanton J. J., Dale D. A., Williams B. F., 2011c, *ArXiv e-prints*
- Weisz D. R., Johnson B. D., Johnson L. C., Skillman E. D., Lee J. C., Kennicutt R. C., Calzetti D., van Zee L., Bothwell M. S., Dalcanton J. J., Dale D. A., Williams B. F., 2012a, *ApJ*, 744, 44
- Weisz D. R., Skillman E. D., Cannon J. M., Walter F., Brinks E., Ott J., Dolphin A. E., 2009, *ApJ*, 691, L59
- Weisz D. R., Zucker D. B., Dolphin A. E., Martin N. F., de Jong J. T. A., Holtzman J. A., Dalcanton J. J., Gilbert K. M., Williams B. F., Bell E. F., Belokurov V., Wyn Evans N., 2012b, *ArXiv e-prints*
- White R. E., Keel W. C., 1992, *Nature*, 359, 129
- White III R. E., Keel W. C., Conselice C. J., 2000, *ApJ*, 542, 761

APPENDIX B: STAR-FORMATION RATIOS FROM HUNTER ET AL 2010

Hunter et al. (2010) provide ratios between the star-formation derived from FUV and those from H α and broad-band V. Figures B2 and B1 show the relations with the $SFR_{FUV}/SFR_{H\alpha}$ and Figures B4 and B3 show the relations with the SFR_{FUV}/SFR_V . Only very weak trends are visible (see also Table 3). Figures B6, B5, B6 and ?? show the direct relations with the H α and V-band star-formation estimates from Hunter et al. (2010) with the H I morphology parameters.

APPENDIX C: VALUES FROM WEISZ ET AL 2011

In addition to a mean star-formation rate, Weisz et al. (2011a) provide a mass-to-light ratio from their stellar populations. Figure C2 shows the ANGST galaxies colour-coded by their M/L ratio and Figure C1 the direct relations but no trend emerges with any of the H I morphological parameters (low values in Table 3). Weisz et al. (2011a) also give the fraction of the stars formed at a given epoch (1, 2, 3, 6, or 10 Gyr ago). Converting these fractions to a mean age, we colour-code the ANGST galaxies with this mean age in Figure C3. There is no relation between the mean stellar age and the distribution of the H I morphology parameters from the VLA-ANGST (Table 3).

**APPENDIX A: THE MORPHOLOGICAL PARAMETERS OF THE H I COLUMN DENSITY MAPS
BASED ON THE RO MAPS FROM LITTLE-THINGS AND VLA-ANGST SURVEYS.**

Name	Gini	M_{20}	$C_{20/80}$	A	S	E	G_M
CVnIdwA	0.596 ± 0.015	-1.582 ± 0.074	2.388 ± 0.135	1.941 ± 0.092	0.046 ± 0.049	0.276 ± 0.027	0.290 ± 0.039
DDO43	0.499 ± 0.013	-1.275 ± 0.060	2.076 ± 0.114	1.793 ± 0.049	0.187 ± 0.043	0.201 ± 0.013	0.320 ± 0.015
DDO46	0.485 ± 0.012	-1.171 ± 0.038	2.014 ± 0.088	1.384 ± 0.050	0.228 ± 0.038	0.079 ± 0.018	0.387 ± 0.017
DDO47	0.399 ± 0.008	-0.948 ± 0.012	1.769 ± 0.036	0.612 ± 0.058	0.107 ± 0.022	0.118 ± 0.009	0.360 ± 0.010
DDO50	0.483 ± 0.007	-1.146 ± 0.015	1.846 ± 0.043	1.742 ± 0.014	0.239 ± 0.020	0.118 ± 0.011	0.396 ± 0.007
DDO52	0.386 ± 0.012	-0.998 ± 0.056	1.838 ± 0.083	1.239 ± 0.159	0.253 ± 0.025	0.337 ± 0.017	0.396 ± 0.014
DDO53	0.535 ± 0.018	-1.323 ± 0.053	2.244 ± 0.119	1.951 ± 0.052	0.192 ± 0.043	0.086 ± 0.030	0.374 ± 0.025
DDO63	0.483 ± 0.013	-1.116 ± 0.029	2.172 ± 0.059	1.449 ± 0.041	0.247 ± 0.030	0.059 ± 0.021	0.438 ± 0.011
DDO69	0.520 ± 0.012	-1.227 ± 0.041	2.287 ± 0.102	1.551 ± 0.154	0.210 ± 0.024	0.477 ± 0.016	0.429 ± 0.011
DDO70	0.414 ± 0.011	-1.461 ± 0.025	2.264 ± 0.055	1.136 ± 0.037	0.057 ± 0.018	0.101 ± 0.015	0.308 ± 0.010
DDO75	0.551 ± 0.006	-0.697 ± 0.001	0.104 ± 0.012	2.000 ± 0.000	0.152 ± 0.025	0.187 ± 0.012	0.552 ± 0.006
DDO87	0.383 ± 0.014	-1.039 ± 0.028	1.808 ± 0.059	0.736 ± 0.066	0.198 ± 0.026	0.158 ± 0.018	0.371 ± 0.016
DDO101	0.356 ± 0.022	-1.003 ± 0.025	1.716 ± 0.144	1.682 ± 0.162	0.238 ± 0.046	0.298 ± 0.030	0.360 ± 0.031
DDO126	0.453 ± 0.018	-1.083 ± 0.061	2.166 ± 0.124	1.360 ± 0.266	0.128 ± 0.045	0.530 ± 0.017	0.464 ± 0.018
DDO133	0.403 ± 0.022	-1.107 ± 0.031	1.940 ± 0.059	1.820 ± 0.091	0.044 ± 0.054	0.196 ± 0.019	0.338 ± 0.020
DDO154	0.524 ± 0.006	-1.479 ± 0.031	2.845 ± 0.110	1.519 ± 0.058	0.201 ± 0.031	0.523 ± 0.013	0.443 ± 0.007
DDO155	0.487 ± 0.017	-1.083 ± 0.057	1.898 ± 0.151	1.481 ± 0.138	0.079 ± 0.040	0.153 ± 0.023	0.335 ± 0.028
DDO165	0.526 ± 0.012	-0.992 ± 0.045	1.795 ± 0.103	1.955 ± 0.055	0.135 ± 0.052	0.360 ± 0.031	0.420 ± 0.018
DDO167	0.480 ± 0.014	-1.303 ± 0.129	2.116 ± 0.212	1.847 ± 0.167	0.187 ± 0.038	0.473 ± 0.018	0.416 ± 0.020
DDO168	0.613 ± 0.009	-1.878 ± 0.057	2.986 ± 0.136	1.137 ± 0.043	0.140 ± 0.052	0.393 ± 0.013	0.383 ± 0.012
DDO187	0.539 ± 0.013	-1.554 ± 0.093	2.397 ± 0.212	1.438 ± 0.238	0.215 ± 0.058	0.248 ± 0.028	0.341 ± 0.022
DDO210	0.509 ± 0.013	-0.699 ± 0.001	0.021 ± 0.003	2.000 ± 0.000	0.089 ± 0.037	0.161 ± 0.055	0.508 ± 0.013
DDO216	0.464 ± 0.019	-1.374 ± 0.113	2.360 ± 0.256	1.688 ± 0.101	0.091 ± 0.073	0.480 ± 0.020	0.383 ± 0.036
F564-V3	0.381 ± 0.013	-1.539 ± 0.113	2.324 ± 0.155	1.670 ± 0.204	0.162 ± 0.024	0.325 ± 0.022	0.305 ± 0.023
IC10	0.483 ± 0.004	-1.525 ± 0.024	2.767 ± 0.033	1.984 ± 0.003	0.346 ± 0.004	0.310 ± 0.005	0.534 ± 0.002
IC1613	0.465 ± 0.008	-1.020 ± 0.024	1.562 ± 0.044	1.076 ± 0.029	0.153 ± 0.021	0.289 ± 0.015	0.391 ± 0.008
LGS3	0.237 ± 0.021	-1.003 ± 0.053	1.948 ± 0.176	1.179 ± 0.092	0.348 ± 0.051	0.317 ± 0.017	0.442 ± 0.015
M81dwA	0.373 ± 0.015	-0.912 ± 0.029	1.251 ± 0.097	2.000 ± 0.000	0.274 ± 0.031	0.116 ± 0.023	0.350 ± 0.019
NGC1569	0.656 ± 0.003	-1.784 ± 0.073	3.118 ± 0.273	1.987 ± 0.002	0.310 ± 0.036	0.294 ± 0.030	0.525 ± 0.005
NGC2366	0.567 ± 0.007	-1.326 ± 0.031	2.437 ± 0.052	1.565 ± 0.084	0.164 ± 0.017	0.533 ± 0.006	0.438 ± 0.005
NGC3738	0.611 ± 0.008	-1.543 ± 0.063	2.531 ± 0.226	1.916 ± 0.019	0.283 ± 0.034	0.317 ± 0.015	0.440 ± 0.007
NGC4163	0.534 ± 0.017	-1.345 ± 0.097	2.249 ± 0.188	1.194 ± 0.224	0.204 ± 0.049	0.091 ± 0.038	0.361 ± 0.020
NGC4214	0.478 ± 0.006	-1.319 ± 0.023	2.143 ± 0.044	0.969 ± 0.040	0.230 ± 0.017	0.167 ± 0.014	0.386 ± 0.008
SagDIG	0.421 ± 0.021	-0.703 ± 0.002	0.068 ± 0.004	2.000 ± 0.000	0.076 ± 0.049	0.175 ± 0.016	0.416 ± 0.021
UGC8508	0.587 ± 0.011	-1.493 ± 0.073	2.736 ± 0.224	1.937 ± 0.073	0.269 ± 0.054	0.584 ± 0.044	0.442 ± 0.014
WLM	0.534 ± 0.005	-0.701 ± 0.003	0.282 ± 0.014	2.000 ± 0.000	0.213 ± 0.018	0.553 ± 0.004	0.540 ± 0.005
Haro29	0.508 ± 0.016	-1.401 ± 0.149	2.419 ± 0.241	0.949 ± 0.088	0.246 ± 0.030	0.199 ± 0.019	0.366 ± 0.018
Haro36	0.597 ± 0.016	-1.615 ± 0.146	2.590 ± 0.177	1.605 ± 0.076	0.176 ± 0.041	0.316 ± 0.018	0.398 ± 0.028
Mrk178	0.500 ± 0.020	-1.362 ± 0.072	2.506 ± 0.292	1.254 ± 0.142	0.226 ± 0.049	0.429 ± 0.020	0.500 ± 0.019
VIIZw403	0.591 ± 0.012	-1.774 ± 0.178	2.714 ± 0.378	2.000 ± 0.000	0.180 ± 0.089	0.464 ± 0.025	0.362 ± 0.018
NGC247	0.344 ± 0.006	-0.698 ± 0.002	0.000 ± 0.004	2.000 ± 0.000	0.061 ± 0.009	... ± 0.002	0.344 ± 0.005
NGC404	0.296 ± 0.005	-0.875 ± 0.011	0.000 ± 0.033	1.434 ± 0.019	0.356 ± 0.013	... ± 0.008	0.456 ± 0.004
UGC4483	0.563 ± 0.014	-1.652 ± 0.128	0.000 ± 0.169	1.946 ± 0.075	0.131 ± 0.039	... ± 0.029	0.283 ± 0.024
SextansB	0.429 ± 0.011	-1.422 ± 0.032	0.000 ± 0.044	0.858 ± 0.071	0.068 ± 0.016	... ± 0.013	0.322 ± 0.013
NGC3109	0.445 ± 0.010	-0.741 ± 0.002	0.000 ± 0.010	2.000 ± 0.000	0.047 ± 0.031	... ± 0.006	0.429 ± 0.011
Antlia	0.281 ± 0.015	-0.703 ± 0.001	0.000 ± 0.004	2.000 ± 0.000	0.229 ± 0.036	... ± 0.019	0.278 ± 0.015
SextansA	0.491 ± 0.009	-0.695 ± 0.002	0.000 ± 0.002	2.000 ± 0.000	0.069 ± 0.021	... ± 0.011	0.490 ± 0.009
DDO82	0.396 ± 0.020	-1.013 ± 0.089	0.000 ± 0.169	1.924 ± 0.053	0.278 ± 0.038	... ± 0.022	0.402 ± 0.031
KDG73	0.224 ± 0.034	-0.780 ± 0.048	0.000 ± 0.377	2.000 ± 0.000	0.423 ± 0.058	... ± 0.014	0.413 ± 0.050
NGC3741	0.392 ± 0.010	-1.752 ± 0.059	0.000 ± 0.079	1.974 ± 0.010	0.143 ± 0.014	... ± 0.006	0.456 ± 0.009
DDO99	0.447 ± 0.010	-1.412 ± 0.035	0.000 ± 0.097	1.903 ± 0.028	0.151 ± 0.028	... ± 0.010	0.375 ± 0.011
NGC4163	0.534 ± 0.013	-1.360 ± 0.083	2.225 ± 0.159	1.281 ± 0.136	0.204 ± 0.055	0.091 ± 0.038	0.351 ± 0.021
MCG9-20-131	0.539 ± 0.016	-1.735 ± 0.146	0.000 ± 0.205	1.033 ± 0.357	0.131 ± 0.057	... ± 0.021	0.277 ± 0.049
UGCA292	0.562 ± 0.019	-1.439 ± 0.104	0.000 ± 0.137	0.984 ± 0.474	0.078 ± 0.051	... ± 0.037	0.308 ± 0.040
GR8	0.441 ± 0.017	-0.982 ± 0.055	0.000 ± 0.108	1.368 ± 0.222	0.105 ± 0.038	... ± 0.015	0.361 ± 0.018
UGC8508	0.587 ± 0.012	-1.493 ± 0.106	2.736 ± 0.185	1.937 ± 0.086	0.269 ± 0.063	0.584 ± 0.033	0.442 ± 0.017
KKH86	0.205 ± 0.032	-0.702 ± 0.058	0.000 ± 0.267	1.995 ± 0.173	0.452 ± 0.079	... ± 0.037	0.410 ± 0.047
UGC8833	0.541 ± 0.022	-1.338 ± 0.113	0.000 ± 0.218	0.543 ± 0.268	0.051 ± 0.045	... ± 0.040	0.249 ± 0.035
KK230	0.361 ± 0.022	-1.162 ± 0.079	0.000 ± 0.195	1.036 ± 0.368	0.220 ± 0.034	... ± 0.015	0.370 ± 0.050
DDO187	0.539 ± 0.011	-1.554 ± 0.128	2.397 ± 0.137	1.438 ± 0.252	0.215 ± 0.044	0.248 ± 0.037	0.341 ± 0.027

Table A1. The morphological parameters of the H I column density maps for the combined LITTLE-THINGS and VLA-ANGST surveys.

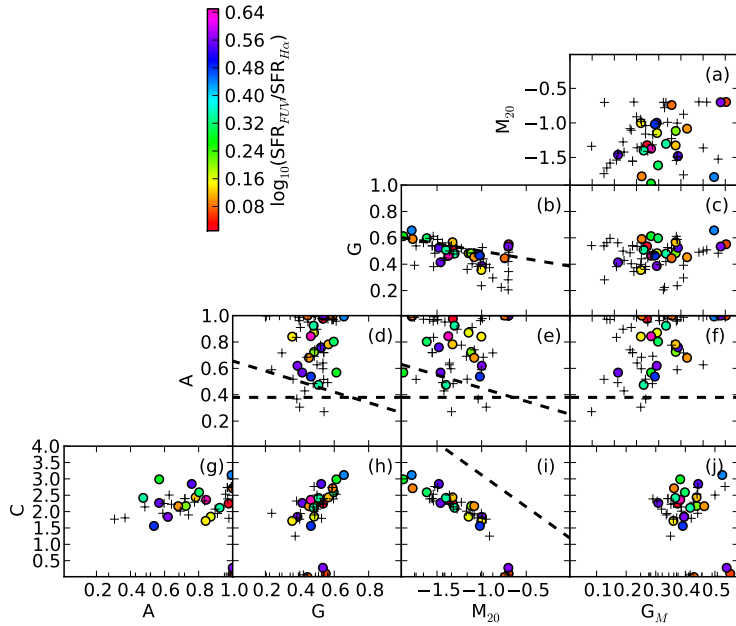


Figure B2. The distribution of the H I morphological parameters colour coded by the ratio of star-formation rate based on FUV/H α from Hunter et al. (2010).

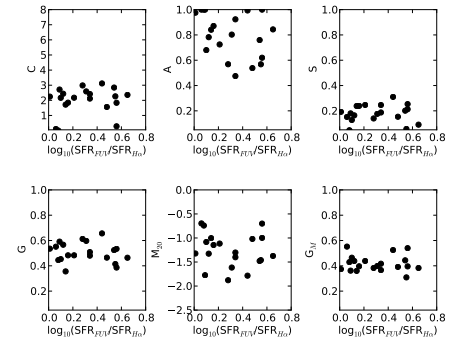


Figure B1. The distribution of the H I morphological parameters versus the ratio of star-formation rate based on FUV/H α from Hunter et al. (2010).

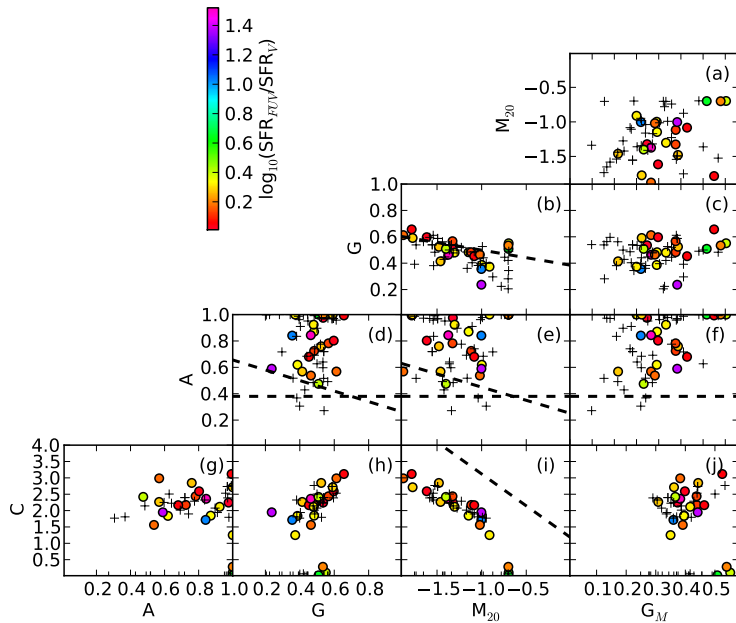


Figure B4. The distribution of the H I morphological parameters colour coded by the ratio of star-formation rate based on FUV/V-band from Hunter et al. (2010).

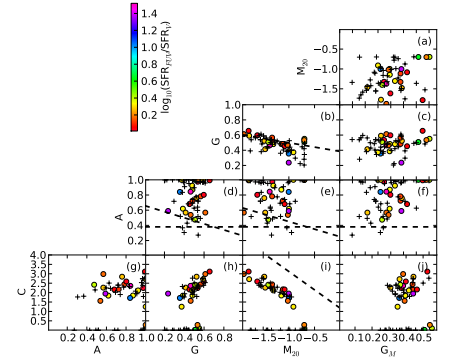


Figure B3. The distribution of the H I morphological parameters versus the ratio of star-formation rate based on FUV/V-band from Hunter et al. (2010).

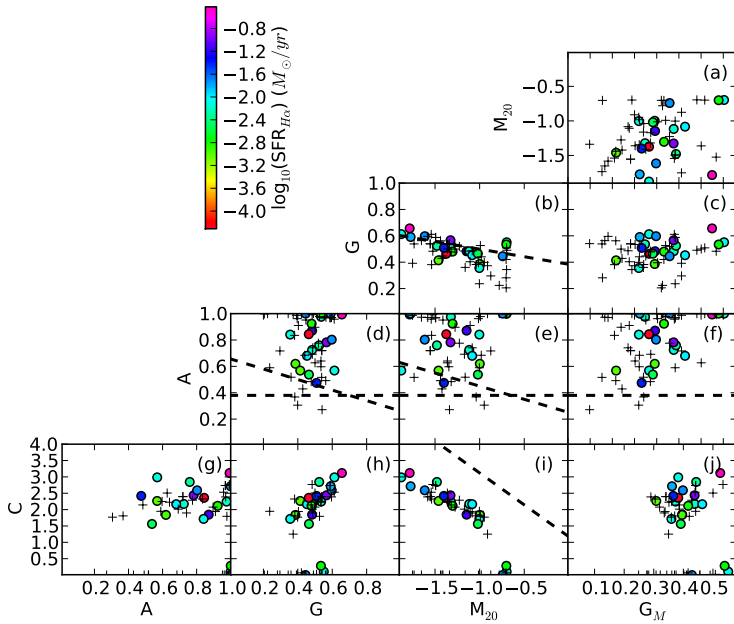


Figure B6. The distribution of the H I morphological parameters colour coded by the star-formation rate based on H α flux reported in Hunter et al. (2010).

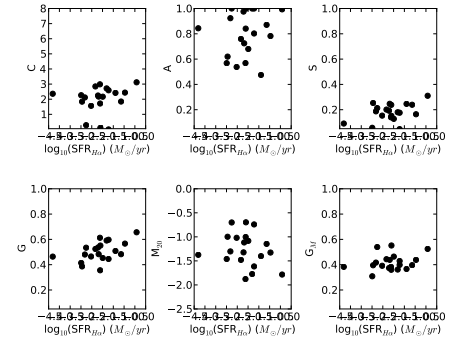


Figure B5. The relation between H α -derived SFR from Hunter et al. (2010) and the six morphology parameters.

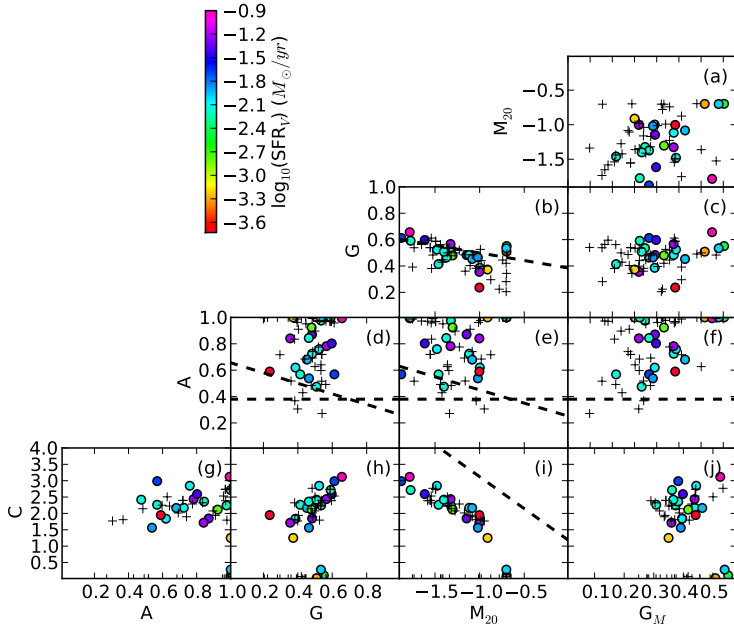


Figure B8. The distribution of the H I morphological parameters colour coded by the star-formation rate based on V-band flux reported in Hunter et al. (2010).

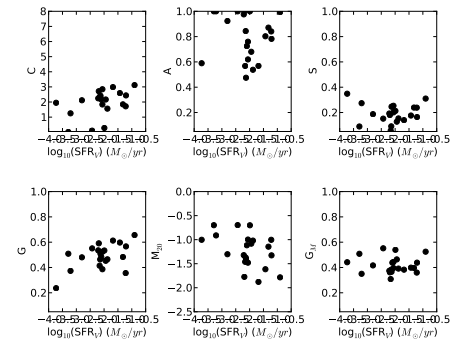


Figure B7. The relation between V-band derived SFR from Hunter et al. (2010) and the six morphology parameters.

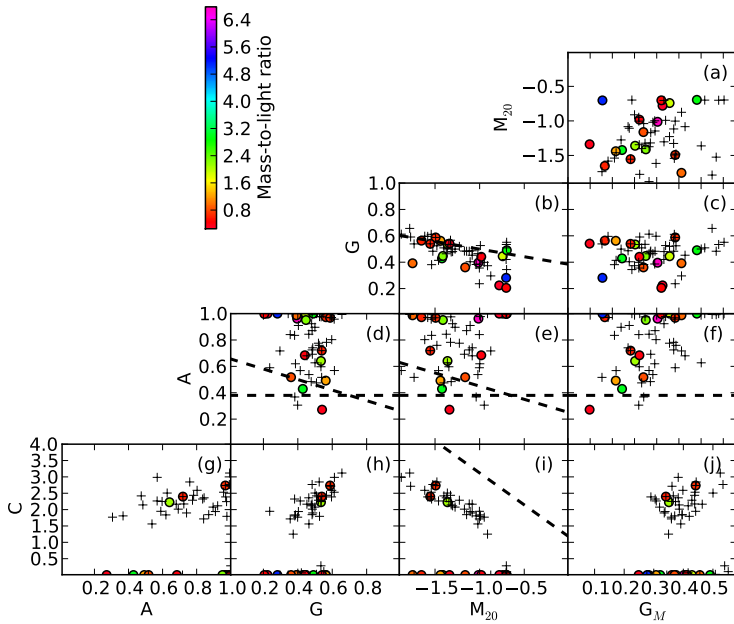


Figure C2. The morphology of the H I maps colour coded by the mass-to-light ratio from Weisz et al. (2011a).

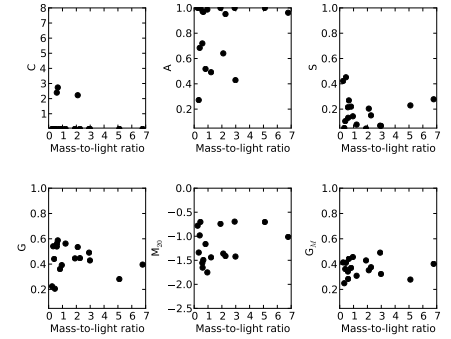


Figure C1. The morphology of the H I maps colour versus the mass-to-light ratio from Weisz et al. (2011a).

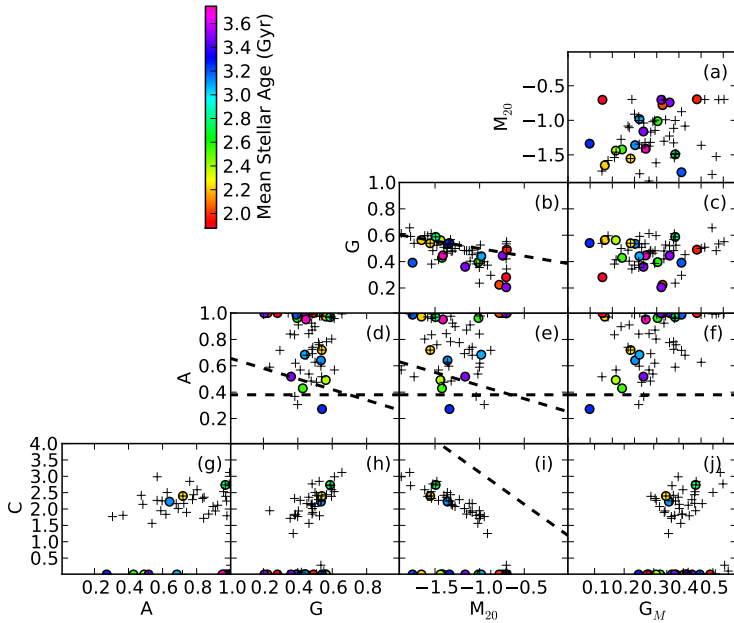


Figure C4. The morphology of the H I maps versus the mean stellar age from Weisz et al. (2011a).

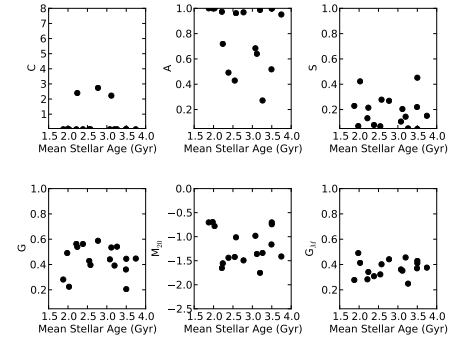


Figure C3. The morphology of the H I maps colour coded by the mean stellar age from Weisz et al. (2011a).